PREPARED FOR THE U.S. DEPARTMENT OF ENERGY,
UNDER CONTRACT DE-AC02-76CH03073

PPPL-3674rev
UC-70

PPPL-3674rev

Fusion Alpha Parameters in Tokamaks with High DT Fusion Rates

by

R.V. Budny

Revised: August 2002

PPPL
PRINCETON PLASMA
PHYSICS LABORATORY

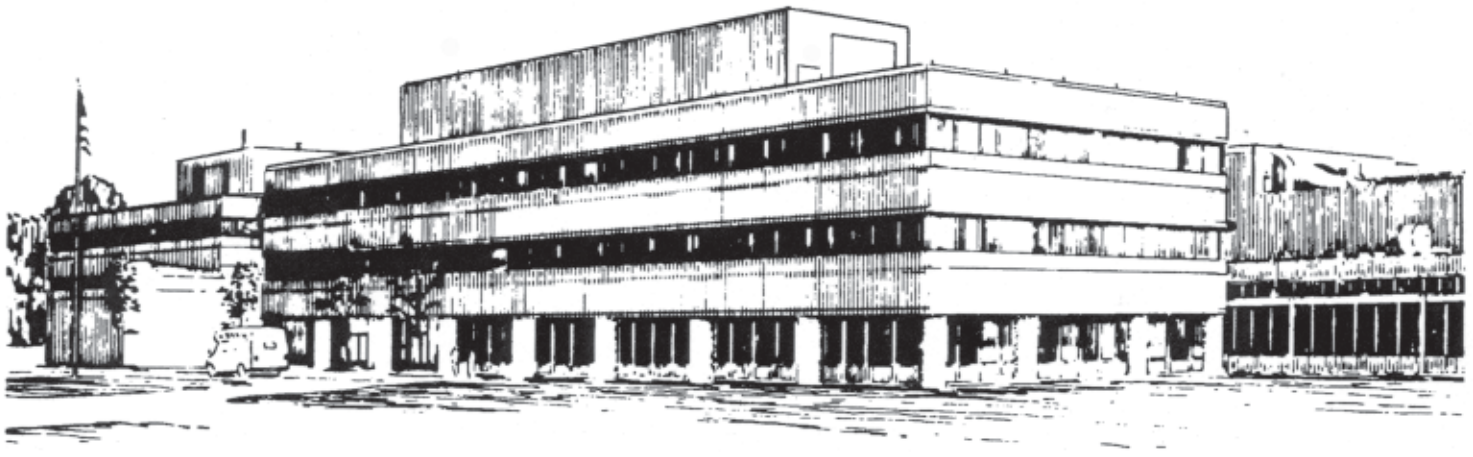

PRINCETON PLASMA PHYSICS LABORATORY
PRINCETON UNIVERSITY, PRINCETON, NEW JERSEY

PPPL Reports Disclaimer

Availability

This report is posted on the U.S. Department of Energy's Princeton Plasma Physics Laboratory Publications and Reports web site in Fiscal Year 2002. The home page for PPPL Reports and Publications is: http://www.pppl.gov/pub_report/

DOE and DOE Contractors can obtain copies of this report from:

U.S. Department of Energy
Office of Scientific and Technical Information
DOE Technical Information Services (DTIS)
P.O. Box 62
Oak Ridge, TN 37831

Telephone: (865) 576-8401

Fax: (865) 576-5728

Email: reports@adonis.osti.gov

This report is available to the general public from:

National Technical Information Service
U.S. Department of Commerce
5285 Port Royal Road
Springfield, VA 22161

Telephone: 1-800-553-6847 or
(703) 605-6000

Fax: (703) 321-8547

Internet: http://www.ntis.gov/ordering.htm

Fusion Alpha Parameters in Tokamaks with High DT Fusion Rates

R.V. Budny[1]

PPPL, Princeton University, P.O. Box 451, Princeton, NJ 08543, USA

(Revised 29-Aug-2002, submitted for publication)

Fusion alpha parameters are calculated for Tokamaks with high DT fusion rates using the TRANSP plasma analysis code. Parameters include the fast alpha density n_α, fast alpha pressure normalized to magnetic field energy β_α, and its normalized gradient $-R \times \nabla(\beta_\alpha)$. The plasma conditions are taken from the plasmas in TFTR and JET with the highest DT fusion rates, and from plasmas in the proposed IGNITOR, FIRE, and ITER-FEAT Tokamaks.

Subject classification: 52.55.Fa (Tokamaks), 52.55.Pi (Fusion products effects), 52.65.Pp (Monte Carlo methods)

1. Introduction

For Tokamaks to become practical sources of energy, large numbers of fusion ions must be confined long enough to heat the plasma. The interactions of fusion alphas on the plasma need to be understood to minimize detrimental effects and exploit beneficial effects. Examples of coupling of fast alphas to the thermal plasma that could be deleterious include stabilization of sawteeth [1,2] and TAE activity [3].

The goal of this paper is to quantify fusion alpha parameters from a selection of proposed "next step" Tokamaks to facilitate future assessments of their effects. The first detailed Monte Carlo calculations for alpha effects in IGNITOR, FIRE, and ITER-FEAT are presented. Self-consistent models of the plasmas including their time evolutions are constructed using the TRANSP plasma analysis code [4]. Profiles of alpha parameters, along with the q_{MHD} profiles and MHD equilibria are being used as inputs to codes such as the NOVA-K [5] and HINST [6] for calculating TAE instability. These results are also of use for codes that calculate the MHD stability and micro-turbulence. Besides the summaries of the alpha parameters given here, electronic files of the MHD equilibria and of the phase space distributions of the fast ions are available.

Another use of these results is in designing experiments to study alpha parameters in burning plasmas. It is likely that auxiliary heating of some form will be used in the next step experiments, but if this generates fast ions (as can ICRH and NBI), these can mask or complicate the measurement of fast alpha effects. One possibility is to abruptly shut off the auxiliary heating in the burning plasma. If the auxiliary ions slow down faster than the alphas, there could be a window of opportunity.

Three proposed Tokamaks are considered, IGNITOR [7-11], FIRE [12], and ITER-FEAT [13,14]. One plasma from each is chosen for analysis. Ion cyclotron heating is assumed for each, with the ICRH frequency tuned to resonate with the first-harmonic of the He^3 ion-cyclotron frequency and the second-harmonic of T ions near the magnetic axis. In addition, negative ion neutral beam injection, NNBI is assumed for ITER-FEAT to heat and drive plasma current.

Present-day experiments have produced modest powers from the DT fusion reaction. TFTR

[1]email: budny@princeton.edu

achieved 10.3 MW [15] and JET achieved 16.0 MW [16]. The identical analysis techniques are applied to these plasmas for comparing their achieved alpha parameters with those that can be expected from the three next step Tokamaks. One advantage of using the same analysis tools for both present-day experiments and future experiments is that the definitions used for parameters such as triangularity are the same, minimizing the semantic ambiguities in extrapolating from present to future experiments.

2. Analysis Techniques

2.1. TRANSP

The TRANSP plasma analysis code [4] is used to analyze the plasmas with the measured or assumed plasma parameters and to calculate the heat deposition profiles. TRANSP is a fixed-boundary code, so the plasma boundary is determined either by measurements in the TFTR and JET cases, or by assuming time evolutions of the major and minor radii, elongation, triangularity, and vertical displacement of the boundary in the cases of IGNITOR, FIRE, and ITER-FEAT. The MHD equilibria are calculated in TRANSP solving the Grad-Shafranov equation. The heat and particle fluxes are calculated from the continuity equations. The fusion ions (and beam ions when NBI is used) are treated using Monte Carlo methods [17] to model their source rates, neoclassical orbits, and slowing-down rates. There are various experimental confirmations of the accuracy of the TRANSP fast alpha calculations [18,19].

The evolution of the q_{MHD} profile is calculated in TRANSP. To model effects of sawteeth, sawteeth crash times are assumed, and the TRANSP sawtooth model is used to helically-mix the plasma current and fast ion profiles at the crash time if $q_{MHD}(0) < 1.0$. Otherwise, poloidal field diffusion is calculated assuming neo-classical resistivity and bootstrap current [20], and driven currents in the case of NBI. The sawteeth simulations resulting from this analysis generally agree well with experimental observations in plasmas, such as L-mode, H-mode, and supershots with monotonic or mildly reversed q_{MHD} profiles. All five plasmas studied have conventional, monotonic q_{MHD} profiles, compared in Fig. 1 versus the toroidal flux variable, $x \equiv \sqrt{\text{normalized toroidal flux}}$, which is roughly equal to r/a. The profile for ITER-FEAT is affected by the assumed 1 MeV NNBI. If the sawtooth model is not invoked, the central values for q_{MHD} are predicted to evolve in time to ≈ 0.7 in IGNITOR and ITER-FEAT. Alternative startup evolutions can keep $q_{MHD} > 1.0$. For the plasma startup assumed for FIRE, $q_{MHD}(0)$ remains above unity for most of the auxiliary heating phase. The values of q_{MHD} at the edge, designated $x = 1$, are at the $x = 0.98$ flux surface. Basic plasma conditions during an approximately steady-state phase of each plasma are summarized in Table 1.

The power radiated by the plasmas is simulated by TRANSP, assuming coronal equilibrium, similar to the techniques in Ref. [21]. The power is separated into bremsstrahlung, line, and cyclotron radiation. The bremsstrahlung and line radiation emission powers are computed using tabulated rate coefficients. The cyclotron radiation power emission is calculated by a simple formula given in Ref. [22]. The predictions for a selected time with approximately steady state

conditions are given in Table 2. In the cases of the TFTR and JET plasmas the measured radiation power emissions are larger than the predictions, and so the measured rates are used in the power balance calculations.

The ICRH power deposition profiles are computed using the SPRUCE full wave, reduced-order package [23] in TRANSP. For the next step Tokamaks, relatively close-fitting antenna are assumed, with a strap separation $\Delta = 30\ cm$. The relative phasing of the straps are assumed to be π. The $k_{\|}$ spectra are assumed to have two values at $\pm\pi/\Delta$. One parameter of special interest is the minority "tail temperature", defined by

$$T_{min} = (2/3)W_{min,\perp}/n_{min} \tag{1}$$

where $W_{min,\perp}$ is the energy density of the RF-resonant ion species in the plane perpendicular to the magnetic field and n_{min} is the density of that ion species. The predicted values of $T_{min}(0)$ are low, comparable to $T_i(0)$ in FIRE and ITER-FEAT. Results are summarized in Table 3.

The accumulation of alpha ash in the next-step Tokamaks is simulated assuming

$$\Gamma_{ash} = (-D_{ash}\nabla n_{ash} + V_{ash}n_{ash})A_{surf}, \tag{2}$$

where A_{surf} is the area of the flux surface at x. The value of D_{ash} is assumed to be constant, and the value of V_{ash} is assumed to be zero, excluding the pessimistic possibility of an inward pinch velocity. The ash density, n_{ash}, is calculated from the local source rate of thermalized fusion alphas and recycling influx from the wall.

The recycling coefficient of the ash, R_{ash}, defined as the ratio of the fluxes entering and exiting the plasma boundary, $\Gamma_{in}(1)/\Gamma_{out}(1)$ is assumed (optimistically) to be low, 20 %, corresponding to good pumping of the ash. Under these assumptions, the ash accumulation in the plasmas does not reduce the simulated DT fusion yield significantly. The ash confinement time is defined by the ratio $\int n_{ash}dV/\Gamma_{ash}$. Generally the effective confinement time is defined as

$$\tau^*_{ash} = \tau_{ash}/(1 - R_{ash}). \tag{3}$$

Results are summarized in Table 4.

The thermal energy confinement and anomalous heat transport coefficients are computed by TRANSP. The energy confinement is calculated from

$$\tau_{E,th} = W_{th}/P_{loss} \tag{4}$$

with $P_{loss} = P_{i,cond} + P_{e,cond} + P_{i,conv} + P_{e,conv} + P_{rad} + P_{cx} = P_{heat} - dW_{th}/dt - P_{misc}$ where P_{heat} is the heating power of the thermal plasma and P_{misc} is heating power that does not couple to the thermal plasma, such as orbit and ripple losses. Results are summarized in Table 5.

2.2. Empirical energy confinement scaling laws

The next step plasmas are very different from present day plasmas in many ways, but comparisons of their performance with empirical scaling laws could be useful for assessing the likelihood of being able to produce the plasmas. Several empirical scaling laws for the thermal energy confinement time give accurate fits to existing data. One such fit for ELMy H-mode plasmas [24] is

$$\tau_{IPB98(y,2)} = 0.144 I_p^{0.93} R^{1.39} a^{0.58} \bar{n}_e^{0.41} B_{Tor}^{0.15} A_h^{0.19} \kappa^{0.78} P^{-0.69} \tag{5}$$

where I_p is the plasma current [MA], $\bar{n}_e$ is the line-averaged electron density [$10^{20}/m^3$], B_{Tor} is the toroidal magnetic field [T], A_h is the volume-averaged isotopic mass of the hydrogenic species, and P, the total heating power, $P_{aux} + P_{Ohmic} + P_\alpha$ [MW]. In the following P_{heat} is used for P, which is lower for the TFTR and JET plasmas which have non-negligible losses of fast ions (shine-through, orbits intercepting objects, stochastic toroidal field ripple, charge-exchange). Thus the definition of $\tau_{ITB98(y,2)}$ used here is slightly higher than the usual definition.

Although the fit $\tau_{IPB98(y,2)}$ is not applicable to TFTR supershots or to the JET Hot-Ion H-mode plasma, it agrees surprisingly well with $\tau_{E,th}$, as seen in Table 5. The fit is more relevant for comparison with the values calculated for the ELMy H-mode plasmas assumed for FIRE and ITER-FEAT plasmas. The estimate of energy confinement time given by the ratio of the total stored energy and the heating power is higher than $\tau_{E,th}$, since all the plasmas contain fast ion contributions to the total energy.

There are other features of ELMy H-mode plasmas that affect their energy confinement. They tend to have higher energy confinement when the triangularity of their boundary, $\delta(1)$, is large, and when their electron density profile is more peaked. They tend to have lower confinement when $\bar{n}_e$ is high (or very low) relative to the Greenwald density defined as $n_{Greenwald} = I_p/(\pi a^2)$ $[MA/m^2]$. An empirical correction factor that accounts for these effects is given in [25]:

$$f = 0.71 + 0.33\delta(1) - 1.58(f_{GW} - 0.63)^2 + 0.58(\bar{n}_e/n_{ped} - 1) \tag{6}$$

where $f_{Greenwald} = \bar{n}_e/n_{GW}$ and n_{ped} is the electron density at the top of the pedestal. The corrected fit for the confinement time is the product $f\ \tau_{IPB98(y,2)}$.

Another parameter listed in Table 5 is the L-mode [24] fit to τ_E for L-mode plasmas:

$$\tau_L = 0.0578 I_p^{0.96} R^{1.89} a^{-0.06} \bar{n}_e^{0.40} B_{Tor}^{0.03} A_h^{0.20} \kappa^{0.64} P^{-0.73} \tag{7}$$

Table 5 shows that τ_L is about $\tau_{IPB(y,2)}$ / 2 for the plasmas considered.

3. Plasma and alpha parameters

3.1. TFTR

The TFTR plasma chosen was a supershot [15] obtained with extensive wall conditioning and injection of Li pellets into the Ohmic phase to reduce the influx of hydrogenic and impurity ions. The auxiliary heating consisted of 25.3 MW of T-NBI, 14 MW of D-NBI, and 0.5 MW Ohmic heating. The plasma experienced a minor disruption late in the flattop, followed by a carbon bloom, probably caused by a flake or limiter dust entering the plasma. This event caused the total number of electrons in the plasma to increase by a factor of 2.6 in 200 msec, increasing f_{GW} from 0.46 to nearly 1.0, while broadening the density profile considerably. With the decreased slowing down time, the alpha heating power increased about 30 % during the bloom, and max$\{P_\alpha/P_{heat}\}$ increased by a factor of three. Due to the need for steady state conditions in a reactor, the parameter values are quoted in Tables 1-5. just before the bloom.

Profiles of the plasma parameters in TFTR before the bloom are shown in Fig. 2. The profile for the anomalous heat conduction, $\chi_{\rm eff}$, rises steeply from the core to the edge, and is near 1.5 [m^2/s] at the mid-radius ($x = 0.5$). Time evolutions of selected plasma parameters are shown

in Fig. 3. Table 5 gives a summary of some parameters of use for quantifying effects of alpha particles such as the slowing down time (for energy to slow to 1.5 T_i) in the center.

3.2. JET

The JET plasma chosen was a hot-ion H-mode [16] achieved by starting with a relatively low-density Ohmically-heated plasma. The auxiliary heating consisted of 11.9 MW D-NBI, 10.5 MW T-NBI, 0.4 MW Ohmic, and 3.2 MW ICRH tuned to resonate with hydrogen-minority ions near the plasma axis. The plasma energy increased throughout an ELM-free period lasting 0.9 s. Then a series of three giant ELMs occurred. The values of the alpha parameters quoted in Table 5 are at 13.35 s, just before the first giant ELM, and the end of the charge-exchange spectroscopy data. Higher values are recorded [26] 100 msec after the first giant ELM; however the giant ELMs do not appear compatible with practical reactors.

Results of the ICRH modeling are summarized in Table 3. Profiles of the plasma parameters just before the first giant ELM are shown in Fig. 4. The profile for $\chi_{\rm eff}$ is relatively flatter than that for the TFTR supershot, and is near 0.4 [m$^2/s$] at the mid-radius. Time evolutions of some of the plasma parameters are shown in Fig. 5.

3.3. IGNITOR

IGNITOR [7-11] is designed to have a high toroidal field with normal-conducting magnets, so the plasma durations will be relatively short. It is not designed to have a divertor, so the plasma boundary will be shaped by limiters. High plasma current and high electron density with a peaked profile are assumed. Some of the plasma parameters differ slightly from those given in Refs. 7-11. Profiles during the flattop are shown in Fig. 6. The limiters are designed to be made of molybdenum, but the dominant impurity species is assumed to be carbon with the Z_{eff} profile shown in Fig. 6. The alpha ash density is also shown. The discharge duration is too short for the alpha ash to obtain steady state. Even if R_{ash} were unity, the accumulation of ash would not reduce P_{DT} significantly.

Although Ohmic ignition is envisioned, the case considered here has 24 MW of He^3-minority ICRH. Two frequencies are assumed, 12 MW at 120 MHz and 12 MW at 140 MHz to place the resonance near the magnetic axis both during the ramp up of the toroidal field, and the flattop. A contour plot of the power deposition is shown in Fig. 7. The value computed for $\tau_{E,th}$ is nearly equal to the L-mode fit, τ_L, and below the ELMy H-mode fit $\tau_{IPB98(y,2)}$. Thus the assumed profiles and heating do not reflect the possibility of a dramatic enhancement of confinement that could result from assumed high values for $n_e(0)$ and peakedness.

The assumed time evolutions for the plasma parameters are shown in Fig. 8. The density and temperature profiles are assumed to rampup slowly in the Ohmic phase, and then rapidly as the ICRH and alpha heating increase in order to keep high (conservative) values for χ_i and χ_e. In contrast, the density and temperature profiles are assumed to rampup in a more steady rate in many of the IGNITOR publications. The assumed startup has little effect on the calculated fusion parameters, which are the focus of this paper. Note that the plasma reaches a steady state so the dW/dt term has a negligible effect in the calculated $\tau_{E,th}$. The computed value for $\chi_{\rm eff}$ is $\approx$ 0.8 [m$^2/s$] near the mid-radius, and higher elsewhere, i.e, more conservative.

To get the same thermal plasma conditions (and alpha parameters) without the additional 24 MW of ICRH the minimum value of $\chi_{\rm eff}$ must be about 0.3 [m^2/s], i.e., more optimistic. The value of $\tau_{E,th}$ would need to be twice the value in Table 5, about 0.53 [s]. This is still considerably lower than the value of $\tau_{IPB98(y,2)} = 0.85s$.

The TRANSP sawtooth mixing model is used to helically-mix the current and fast ions at a sawtooth period of 1 sec. This clamps $q_{MHD}(0)$ to remain near 1.0. With the plasma startup assumed here, the central q_{MHD} would evolve to 0.7 if the sawtooth model were turned off. The sawtooth mixing of the fast alpha particles reduces the alpha parameters in the center, as seen in Fig. 8c. Even though the mixing radius is relatively large, the central alpha heating and alpha density recovers very rapidly.

3.4. FIRE

FIRE [12] is designed to have normal-conducting magnets, and a double-null divertor geometry. The plasma is assumed to operate in the standard ELMy H-mode regime. Profiles of the plasma parameters are shown in Fig. 9. These are based on predictions from the TSC code [27].

Since the divertors are designed to be coated with beryllium, the dominant impurity species, besides the He ash, is assumed to be Be with the Z_{eff} profile shown in the Figure. Accumulation of alpha ash is modeled assuming the ash has an anomalous diffusivity of 0.1 m^2/s with no pinch term. With the computed alpha thermalization rate and wall recycling rate (20%), the ash accumulates to the steady state profile shown in Fig. 9, which has little impact on the fusion rate. If R_{ash} were unity, the predicted P_{DT} would decrease 13% from the peak rate within 12 s. Aggressive pumping may be needed to keep the ash recycling low. The confinement time of the ash is computed to be 1.2 s near the plasma boundary.

The plasma is heated with ICRH at a frequency of 100 MHz to resonate with He^3 on axis. The P_{RF} is 20 MW early, and lowered to 11 MW as the alpha heating increases, to keep $P_\alpha + P_{ext}$ roughly constant. A contour plot of the power deposition and antenna position is shown in Fig. 10.

The computed value for $\tau_{th,E}$ equals $\tau_{IPB98(y,2)}$, but the enhancement factor given in Eq.(6) would increase $\tau_{IPB98(y,2)}$ by a factor of 1.6. The computed value for $\chi_{\rm eff}$ is near 0.34 [m^2/s] near $x = 0.8$, and higher elsewhere. The assumed time evolutions of plasma parameters are shown in Fig. 11.

3.5. ITER-FEAT

ITER-FEAT [13,14] is designed to have super-conducting magnets for long pulse duration, and a single-null divertor geometry. The plasma is assumed to be in the ELMy H-mode regime with profiles close to those in Ref. [14] with a target DT fusion yield of $P_{DT} = 400$ [MW]. Profiles of the plasma parameters are shown in Fig. 12. The profile of T_e in Ref. 14 is about 20% higher than that of T_i. TRANSP computes the thermal ion heating at 180s to be 38 [MW] and the thermal electron heating to be 76 [MW]. Their total is given in Table 2. The density is sufficiently high that the electron-ion energy transfer rate is 51 [MW]. Thus the computed $\chi_{\rm e}$ is low compared to $\chi_{\rm i}$, especially at large radii. This is reflected in $P_{i,cond}(0.9) >> P_{e,cond}(0.9)$ in Table 2.

Accumulation of alpha ash is modeled assuming the ash has an anomalous diffusivity of 0.8 m^2/s with no pinch. With the computed alpha thermalization rate and wall recycling rate (20%), the ash accumulates to the steady state profile shown in Fig. 12, which has little impact of depletion on the fusion rate. The confinement time of the ash near the plasma boundary is computed to be 1.6 s.

The boundary of the plasma is grown from circular to an up/down asymmetric shape, shown in Fig. 13. The assumed ICRH antenna position and computed contours of the induced E_z are shown in Fig. 14. Time evolutions of plasma parameters are shown in Fig. 15. The sawtooth period is assumed to be 10 s.

The external heating is assumed to consist of 20 MW of ICRH staggered with 33 MW of NNBI. This staggering allows study of the heat fluxes and fast ion parameters in three cases with the same assumed plasma profiles: RF-only, RF+NB, and NB-only. The NNBI is assumed to consist of 1 MeV (D or T) neutrals from a negative ion-beam system injected in the co-plasma current direction, at a tangency radius of 6 m. This generates a beam-driven current profile that is broad with a total driven current of 1.2 MA. The bootstrap current profile is large near the edge. The effects of these currents on the q_{MHD} profile were shown in Fig. 1.

During the NNBI the ratio of the beam and fast alpha density is near unity in the center and increases to 20 near the edge. The average energy of the beam ions in the core is 0.4 MeV, about one-third that of the fast alphas. The slowing down time for the beam ions in the center is 1.15 s, longer than $\tau_{slow}(0)$ of the fast alpha particles. This indicates that the NNBI could interfere with attempts to measure alpha parameters. An example of the distribution of the beam ions in energy and pitch angle at $x = 0.45$, averaged over poloidal angle, is shown in Fig. 16.

The ICRH is assumed to be 53 MHz for He^3 resonance on axis. The ICRH minority He^3 ions will not have high energy, and thus should not be a complication in studying fast alpha effects (and will not contribute significantly to stabilizing sawteeth or TAE). Their tail temperature, $T_{min}(0)$ is close to T_i, as shown in Table 3.

The value of $\tau_{E,th}$ is slightly below the $\tau_{IPB98(y,2)}$ value. With the choice of a flat n_e profile, the form factor in Eq.(6) reduces $\tau_{E,th}$ by a factor of 0.81. Since the profiles are held fixed during the flattop phase as the heating power changes, the computed $\chi_{\rm eff}$ values change. The minimum value during the phase of maximum heating (20 MW ICRH, 33 MW NNBI, and 75 MW alpha) is 0.7 $[m^2/s]$. The minimum drops to a less optimistic value of 0.5 $[m^2/s]$ after the ICRH is shut off and later to an even more optimistic 0.35 $[m^2/s]$ after the NNBI is shut off. If $\chi_{\rm eff}$ were held constant in time, the stored energy would change as the heating changed.

Alpha parameters have been calculated [28] for two ITER-EDA plasmas producing 1.5 GW fusion power. One had a nearly flat electron density profile, similar to the one used here for ITER-FEAT. The other had a relatively peaked n_e. The values for the alpha parameters calculated in the flat profile case are very similar to those given in Table 5.

4. Summary and Discussion

This paper reports results from TRANSP analysis of five plasmas with high DT fusion yield. The TFTR and JET plasmas with the highest values of P_{DT} obtained so far help to establish

the scientific feasibility of energy production in future Tokamak reactors. Three examples of plasmas from the proposed next step Tokamaks with much higher P_{DT} are analyzed. The plasma startup and steady state phases are modeled self-consistently, including auxiliary heating and accumulation of alpha ash. The results of this study include electronic files of the MHD equilibria, plasma parameters, and alpha parameters, including distributions in energy and patch angle are available for use in studies of alpha effects and MHD and microturbulence instabilities.

The assumed plasma conditions for FIRE and ITER-FEAT are similar to examples proposed by their proponents. The assumed plasma conditions for IGNITOR differ is some inconsequential details from examples proposed by it's proponents. These assumed plasma profiles and computed heat deposition profiles give values of $\tau_{E,th}$ close to the L-mode scaling in the case of IGNITOR and close to the ELMy H-mode fits in Eqs. (5, 6) in the cases of FIRE and ITER-FEAT. It would be useful to use physics-based and empirical models to predict plasma profiles that can be sustained by the heating and fueling sources.

Examples of results are the predictions 1) that if sawteeth occur in IGNITOR, they will not have adverse effects on the alpha parameters, 2) that pumping of the alpha ash will be needed in FIRE (and of course in ITER) to maintain high P_{DT}, 3) that the He^3 minority ions will not be accelerated by ICRH to energies much above T_i in FIRE and ITER, and 4) that the NNBI ions will complicate measurement of fast alphas in ITER. The result 3) suggests that ICRH will not complicate measurements of fast alphas, and thus high fusion energy gain Q is not necessary for such measurements.

There are a number of interesting similarities and expected differences between the TFTR and JET plasmas and those considered for the next step burning plasma experiments in IGNITOR, FIRE, and ITER. Similarities include the values of $\beta_\alpha(0), v_\alpha(0)/v_{Alfven}(0)$, and $\max\{-R \times \nabla(\beta_\alpha)\}$, which vary by a factor of at most four for the five plasmas. The value of $\max\{P_\alpha/P_{heat}\}$ varies by only a factor of 4.5. Steady-state profiles of the fast alpha density in IGNITOR, FIRE, and ITER-FEAT are expected to be vary similar, as shown in Fig. 17. Steady-state profiles of $-R \times \nabla(\beta_\alpha)$ in IGNITOR, FIRE, and ITER-FEAT are shown in Fig. 18.

One major difference is that $T_i >> T_e$ in the core of the TFTR and JET plasmas, whereas they are assumed and expected to be nearly equal in the next step Tokamak plasmas since the energy equilibration should be fast at higher density. Another difference is that the TFTR and JET plasmas have large toroidal rotation rates due to the intense NBI (with central Mach numbers of the carbon impurity being 0.25 and 1.6 respectively), whereas the next step plasmas are expected to have very low rotation rates due to the difficulty (cost) of injecting momentum into a Tokamak reactor. Both $T_i >> T_e$ and large rotation rates are correlated with high confinement in present-day experiments. Another difference is that the slowing down times for the alpha particles (τ_{slow}) is small compared to the thermal energy confinement times in the burning plasmas, unlike the situation in the achieved experiments.

Issues for future investigation include using models to predict the temperature profiles, and checking the MHD and micro-instability of the plasmas. Several predictive transport models such as the multi-mode [29] and GLF23 [30] models have been incorporated into TRANSP, and could be used to predict the temperature profiles. The instability to ITG modes depends sensitively on the temperature gradients. If the plasmas are unstable, the pedestal temperatures

may have to be increased to reduce the gradients while keeping the central values high enough for high P_{DT}. However, it appears that the temperature at the separatrix should be well below 1 [keV] to prevent excessive sputtering erosion of surfaces down stream in the divertor [31]. These constraints suggest the need for a large decrease in T_i between the top and bottom of the pedestal. Experiments in JET suggest that if there is in fact a large decrease in the pedestal, the ELMs would be Type I with excessive losses of energy in each ELM [32]. Gyrokinetic analysis of JET ELMy H-mode plasmas indicates that when the flow shear and linear microturbulence growth rates near the top of the pedestal are comparable, the energy confinement remains good [33]. This suggests that driving large flow shear near the top of the pedestal in next step Tokamaks might permit high confinement and central temperatures with low pedestal temperatures.

5. Acknowledgments

This work was supported in part by the US DoE Contract No. DE-AC02-76CH03073. The author wishes to thank the TRANSP development team for providing excellent analysis tools and the TFTR and JET teams for providing excellent plasmas.

Tokamak:		TFTR	JET	IGNITOR	FIRE	ITER
RUNID		80539A24	42976C10	30000B22	50000A26	03000A24
steady state time	[s]	3.76	13.35	6.5	20.0	180.0
R(1)	[m]	2.52	2.92	1.32	2.14	6.2
$R_{Shaf}(0)$	[cm]	17.5	8.0	2.7	3.2	15.4
a(1)	[m]	0.87	0.94	0.48	0.60	2.0
$\kappa(1)$		1.02	1.80	1.80	2.00	1.85
$\delta(1)$		0.02	0.35	0.40	0.49	0.50
$P_{vol}(1)$	$[m^3]$	38.8	84.0	9.9	27.2	820
B_{Tor}	[T]	5.5	3.5	13.0	10.0	5.3
$B_{Pol}(1)$	[T]	0.6	0.5	2.5	1.35	0.85
I_p	[MA]	2.7	4.0	11.0	7.7	15.0
I_{beam}	[MA]	0.05	0.18	N/A	N/A	1.2
I_{boot}	[MA]	0.65	0.40	1.0	1.8	3.0
$q_{MHD}(1)$		4.05	4.7	3.6	4.0	3.8
$T_e(0)$	[keV]	13.2	11.0	9.9	11.9	23.5
$< T_e >$	[keV]	8.7	7.3	5.2	7.2	10.0
$T_i(0)$	[keV]	41.0	23.0	9.9	11.9	19.5
$< T_i >$	[keV]	8.7	7.3	5.2	7.2	8.6
A_h		2.20	2.53	2.5	2.5	2.5
$n_e(0)$	$[10^{20}/m^3]$	1.02	0.45	9.4	4.9	1.02
$\bar{n}_e$	$[10^{20}/m^3]$	0.51	0.46	5.3	4.0	1.00
$< n_e >$	$[10^{20}/m^3]$	0.40	0.48	3.3	3.4	0.98
$\bar{n}_e/\bar{n}_{Greenwald}$		0.46	0.32	0.35	0.59	0.84
A_{imp}		12.4	12.0	12.0	8.0	8.0
Z_{imp}		6.2	6.0	6.0	4.0	4.0
$Z_{eff}(0)$		3.1	1.5	1.2	1.39	1.54
$n_{imp}(0)/n_e(0)$	%	5.5	1.5	0.5	2.7	3.9

Table 1. *Summary of boundary and plasma parameters at a steady state time. All the parameters are inputs except the Shafranov shift of the magnetic axis $R_{Shaf}(0)$, I_{boot} (calculated using the NCLASS code [20]), B_{Pol}, I_{beam}, q_{MHD} (calculated accounting for poloidal field diffusion). The time-evolving geometry of the boundary (x=1) is specified. A_{imp} and Z_{imp} are chosen as the atomic mass and charge of an effective impurity ion whose density profiles are determined by the assumed (or in the cases of TFTR and JET measured) Z_{eff} profiles after the computed helium ash contribution is subtracted.*

Tokamak:		TFTR	JET	IGNITOR	FIRE	ITER
RUNID		80539A24	42976C10	30000B22	50000A26	03000A24
steady state time	[s]	3.76	13.35	6.5	20.0	180.0
P_{Ohmic}	[MW]	0.5	0.4	6.0	1.3	1.1
P_{NB}	[MW]	39.3	22.4	0.0	0.0	33.0
P_{RF}	[MW]	0.0	3.2	24.0	11.2	early
P_{ext}	[MW]	40.8	26.0	30.0	12.5	34.1
P_{DT}	[MW]	9.5	15.7	75.1	149	400
$P_{\alpha-el}$	[MW]	1.1	2.1	12.4	24.0	57
$P_{\alpha-ion}$	[MW]	0.1	0.3	2.6	5.6	22
P_{α}	[MW]	1.2	2.4	15.0	29.6	80
$P_{ext} + P_{\alpha}$	[MW]	42.0	28.4	45.0	42.0	114
P_{heat}	[MW]	27.0	16.4	44.6	42.1	114
$P_{i,cond}(0.9)$	[MW]	11.0	10.1	19.0	13.2	90.0
$P_{i,conv}(0.9)$	[MW]	2.0	7.5	0.1	0.6	0.9
$P_{e,cond}(0.9)$	[MW]	7.0	0.0	20.5	19.0	3.0
$P_{e,conv}(0.9)$	[MW]	0.0	1.0	0.1	0.5	0.4
P_{brem}	[MW]	0.3	0.6	3.4	8.2	21.0
P_{line}	[MW]	0.1	0.1	0.4	0.1	4.0
P_{cyc}	[MW]	0.1	0.1	0.1	0.02	0.6
P_{rad}	[MW]	3.2	3.3	4.1	9.0	26.0
P_{cx}	[MW]	0.5	9.2	0.1	2.0	0.8

Table 2. *Heating and heat loss rates at the steady state times used in Table 1. P_{heat} is the total heating power of the thermal plasma calculated by TRANSP. The conduction and convection losses are given at the $x = 0.9$ surface since they vary only weakly near that surface, but rapidly at larger radii. The P_{brem}, and P_{line} contributions to P_{rad} are computed in TRANSP using a coronal equilibrium model. The P_{cyc} contribution to P_{rad} is computed using a simple estimate. The values for P_{rad} measured in TFTR and JET are considerably higher than the sum $P_{brem} + P_{rad} + P_{cyc}$. Several explanations could account for this: 1) these plasmas are not in coronal equilibria, 2) small amounts of high Z impurities are contributing, or 3) the bolometry measurements of P_{rad} are wrong (for instance, they could be measuring charge-exchange particles as well as photons).*

Tokamak:		JET	IGNITOR	FIRE	ITER
RUNID		42976C10	30000B23	50000A28	03000A24
time	[s]	13.35	6.5	20.0	140.0
Ω_{RF}	[MHz]	51.2-56.5	120/140	100	53
P_{RF}	[MW]	3.4	12/12	11	20
minority ion		H	He^3	He^3	He^3
n_{min}/n_e	(%)	2.0	2.0	2.0	3.0
$T_{min}(0)$	[keV]	150	≈130	10.0	28.0
P_{RF-min}/P_{RF}	(%)	60	61/47	62	45
P_{RF-T}/P_{RF}	(%)	1	11/14	10	4
P_{RF-D}/P_{RF}	(%)	17	6/11	2	3
$P_{RF-\alpha}/P_{RF}$	(%)	0	0/3	1	0
P_{RF-e}/P_{RF}	(%)	13	22/23	24	48

Table 3. *Summary of ICRH parameters. The ICRH frequencies Ω_{RF}, powers P_{RF}, and minority ion profiles, n_{min} are assumed. The computed RF minority tail temperature T_{min} is defined in Eq.(1). The fractions of the heating power transferred directly to the minority ion and to the plasma species are calculated in TRANSP using SPRUCE [23]. The transfer of energy from the fast minority ions to the thermal plasma is calculated by TRANSP. For IGNITOR with ICRH at both 120 and 140 GHz, the heating fractions of each are given. Very small concentrations of certain impurities could cause resonances and power absorption far from the magnetic axis and change the power fractions. For instance, with the assumed Ω_{RF} and B_{Tor} for ITER, very small amounts of boron could resonate near the outer edge, absorbing much of P_{RF}.*

Tokamak:		IGNITOR	FIRE	ITER
RUNID		30000B22	50000A26	03000A24
time	[s]	6.5	20.0	180.0
R_{ash}	(%)	20	20	20
D_{ash}	[m^2/s]	0.1	0.1	0.8
$\tau_{ash}(0.95)$	[s]	23.0	1.25	1.55
$n_{ash}(0)/n_e(0)$	(%)	0.9	1.2	0.7

Table 4. *Summary of alpha ash parameters. The diffusivity of the He ash D_{ash} and the recycling coefficient at the boundary R_{ash} are assumed. The time evolutions of the profiles of the confinement time defined in Eq.(2) and the ash density are calculated by TRANSP. These are in steady state for the FIRE and ITER plasmas.*

Tokamak:	TFTR	JET	IGNITOR	FIRE	ITER
RUNID	80539A24	42976C10	30000B22	50000A26	03000A24
steady state time [s]	3.76	13.35	6.5	20.0	180.0
$< \beta_{total} >$ (%)	1.03	2.17	1.10	2.10	2.55
$\beta_{total}(0)$ (%)	6.0	4.9	4.7	4.6	6.5
$< \beta_{thermal} >$ (%)	0.60	1.79	1.05	2.02	2.41
β_{Pol}	0.51	0.94	0.24	0.95	0.85
β_n	1.85	1.95	0.62	1.64	1.85
W_{tot} [MJ]	7.5	17.0	11.4	35.0	360
$W_{tot}/(P_\alpha + P_{ext})$ [sec]	0.18	0.61	0.25	0.83	3.16
$\tau_{E,th}$ [sec]	0.13	0.59	0.25	0.80	2.98
$\tau_{IPB98(y,2)}$ [sec]	0.14	0.55	0.51	0.80	3.15
τ_L [sec]	0.066	0.30	0.23	0.41	1.40
$\tau_{slow}(0)$ [sec]	0.48	1.0	0.042	0.097	0.85
$\tau_{scat}(0)$ [sec]	5.8	21	1.5	2.5	10.8
$P_\alpha(0)$ [MW/m^3]	0.28	0.08	15.0	5.0	0.55
$\max\{P_\alpha/P_{heat}\}$	0.20	0.23	0.65	0.76	0.98
$n_{beam}(0.4)/n_e(0.4)$ %	32.0	8.0	N/A	N/A	0.40
$n_\alpha(0)/n_e(0)$ (%)	0.17	0.28	0.13	0.19	0.85
$\beta_\alpha(0)$ (%)	0.30	0.4	0.23	0.30	1.20
$< \beta_\alpha >$ (%)	0.034	0.1	0.031	0.030	1.30
$max\{-R \times \nabla(\beta_\alpha)\}$ (%)	2.0	2.3	0.8	1.3	4.0
$v_\alpha(0)/v_{Alfven}(0)$	1.72	1.52	2.10	2.10	1.86

Table 5. *Examples of calculated plasma parameters at the steady state times used in Tables 1 and 2. Here β_{Pol} is defined as $p/(8\pi < B_{Pol}^2 >$ where p is the total pressure and $< B_{Pol}^2 >$ is the differential volume average of the poloidal field squared, over the outermost flux surface. The maximum value for P_α/P_{heat} occurs at the magnetic axis for all but FIRE. The maximum value for $-R \times \nabla(\beta_\alpha)$ occurs around $x = 0.30 - 0.45$, as shown in Fig. 18*

References

[1] C. Angioni, A. Pochelon, N.N. Gorelenkov, *et al.***, Plasma Phys. and Cont. Fusion, 44 (2002) 205.**

[2] F. Porcelli, D. Boucher, and M.N. Rosenbluth, PPCF 38 (1996) 2163.

[3] G.F. Fu, C.Z. Chen, N. Gorelenkov, *et al.***, Phys. of Plasmas, 3 (1996) 4036.**

[4] R.V. Budny, M.G. Bell, A.C. Janos, *et al.***, Nucl. Fusion 35 (1995) 1497, and references therein.**

[5] G.Y. Fu, C.Z. Chang, and K.L. Wong, Phys. of Fluids B5 (1993) 4040.

[6] N. Gorelenkov, C.Z. Chang, and W.M. Tang, Phys. of Plasmas 5 (1998) 3389.

[7] A web site for IGNITOR is http://www.frascati.enea.it/ignitor/.

[8] W. Horton, *et al.***, Nucl. Fusion 42 (2002) 169.**

[9] A. Airoldi, G. Cenacchi, Nucl. Fusion 41 (2001) 687.

[10] B. Coppi, A. Aroldi, F. Bombarda, *et al.*, Nucl. Fusion 41 (2001) 1253.
[11] A. Airoldi, G. Cenacchi, Nucl. Fusion 37 (1997) 1117.
[12] D. Meade *et al.*, 2001 Fusion Energy 2000 (Proc. 18th Int. Conf., Sorrento, 2000) (Vienna:IAEA) CD-ROM file FTP2/16 and http://www.iaea.org/programmes/ripc/physics/fec2000/html/node1.htm. A web site for FIRE is http://fire.pppl.gov.
[13] http://www.itereu.de
[14] D.J. Campbell, Phys. Plasmas 8 (2001) 2041.
[15] R. Hawryluk, Rev. Modern Phys., 70 (1998) 537.
[16] M. Keilhacker, A. Gibson, C. Gormezano, P.J. Lomas, *et al.*, Nucl. Fusion 39 (1999) 209.
[17] R.J. Goldston, D.C. McCune, H.H. Towner, S.L. Davis, *et al.*, J. Comput. Phys. 43 (1981) 61.
[18] S.S. Medley, R.V. Budny, H.H. Duong, R.K. Fisher, *et al.*, Nucl. Fusion 38 (1998) 1283.
[19] G.A. McKee, R.J. Fonck, B.C. Stratton, R.V. Budny, Z. Chang, and A.T Ramsey, Nucl. Fusion 37 (1997) 501.
[20] W. Houlberg, K. Shang, S. Hirshman, and M. Zarnstorff, Phys. Plasmas 4 (1997) 3230.
[21] D.E. Post, R.V. Jensen, C.B. Tarter, W.H. Grasberger, and W.A. Lokke, At. Data Nucl. Data tables, 20 (1977) 397.
[22] J.Sheffield in "Tokamak Start-up", H.Knoepfel, editor, Plenum Press 1985, p11.
[23] M. Evrard, J. Ongena, and D. van Eester, "Improved Dielectric Tensor in the ICRH module of TRANSP", in AIP Conference Proceedings 335, Radio-Frequency Power in Plasmas, 11th topical conference, Palm Springs (1995) 235.
[24] ITER Physics Basis, Nucl. Fusion 39 (1999) 2137; see 2204-2208.
[25] J.G. Cordey, D.C. McDonald, K. Borrass, *et al.*, P3.011 in Proc. 28th EPS Conference on Controlled Fusion and Plasma Physics, Madeira, Portugal, 2001. ECA 25A, 969.
[26] S.E. Sharapov, D. Borba, A. Fasoli, *et al.,* Nucl. Fusion 39 (1999) 373.
[27] S.C. Jardin, N. Pomphrey, and J. Delucia, J. Comput. Phys., 46 (1986) 481.
[28] R.V. Budny, D.C. McCune, M.H. Redi, *et al.,* Phys. of Plasmas 3 (1996) 4583.
[29] G. Bateman, A.H. Kritz, J.E. Kinsey, A.J. Redd, and J. Weiland, Phys. Plasmas, 5 (1998) 1793.
[30] R.E. Waltz, G.M. Staebler, W. Dorland, G.W. Hammett, *et al.*, Phys. Plasmas 4 (1997) 2482.
[31] P.C. Stangeby, The Plasma Boundary of Magnetic Fusion Devices, Institute of Physics Publishing (Bristol and Philadelphia, 2000)p 232.
[32] A. Loarte, M. Bécoulet, G. Saibene, *et al.*, P3.005, Proceedings of the 28th EPS conference, Madeira, 2001, ECA 25A, 945.
[33] R.V. Budny, B. Alper, D.N. Borba, J.G. Cordey, *et al.*, Nucl. Fusion, 42 (2002) 66.

Figure Captions

Fig. 1 - Profiles of q_{MHD} in the TFTR, JET, IGNITOR, FIRE, and ITER plasmas during the steady state phases.

Fig. 2 - Profiles of the TFTR supershot before the carbon bloom.

Fig. 3 - Time evolution of parameters in the TFTR supershot. The charge-exchange-measured T_i profile (for carbon) became hollow with unrealistically low central values after the density became too high for good beam penetration. $P_{fast\ ion}$ is the heating power of the thermal plasma from the NBI and alphas. E_α is the average energy of the fast alphas in the core. The alpha parameters in c) are volume-averaged out to the $x = 0.1$ flux surface to reduce Monte Carlo fluctuations. The vertical dashed lines indicate the time of the profiles in Fig. 2 (3.76 s).

Fig. 4 - Profiles of the JET hot-ion H-mode plasma before the series of giant ELMs.

Fig. 5 - Time evolution of parameters in the JET plasma. The vertical dashed lines indicate the time of the profiles in Fig. 4 (14.35 s).

Fig. 6 - Profiles of the IGNITOR plasma in the flattop phase. The He^4 ash density times 100 is computed from the fast alpha thermalization assuming R_{ash} = 20% and D_{ash} = 0.1 $[m^2/s]$.

Fig. 7 - Contours of the 120MHz ICRH-induced Re$\{E_r\}$ in the IGNITOR plasma.

Fig. 8 - Time evolution of parameters in the IGNITOR plasma.

Fig. 9 - Profiles of the FIRE plasma in the flattop phase. The He^4 ash density times 100 is computed from the fast alpha thermalization assuming R_{ash} = 20% and D_{ash} = 0.1 $[m^2/s]$, and is in steady state at the time shown.

Fig.10 - Contours of ICRH-induced Re$\{E_r\}$ in the FIRE plasma.

Fig.11 - Time evolution of parameters in the FIRE plasma. P_{RF} is high early to obtain the L-H mode transition, then is reduced.

Fig.12 - Profiles of the ITER plasma. The He^4 ash density times 100 is computed from the fast alpha thermalization assuming R_{ash} = 20% and D_{ash} = 0.8 $[m^2/s]$, and is in steady state at the time shown.

Fig.13 - Assumed boundary for the ITER plasma

Fig.14 - Contours of the ICRH-induced Re$\{E_r\}$ in ITER-FEAT

Fig.15 - Time evolution of parameters in the ITER plasma. The alpha parameters in c) are volume-averaged out to the $x = 0.1$ flux surface to reduce Monte Carlo fluctuations.

Fig.16 - Distribution of the ITER NNBI beam ions in energy and pitch angle at $x = 0.35$, averaged over poloidal angle, computed by the TRANSP Monte Carlo model. The neutrals are injected at 1MeV with $v_\parallel/v = 1$, and the beam ions become more isotropic as they slow down.

Fig.17 - Profiles of the fast alpha densities in IGNITOR, FIRE, and ITER-FEAT during the steady state phase.

Fig.18 - Profiles of $-R \times \nabla(\beta_\alpha)$ in IGNITOR, FIRE, and ITER-FEAT during the steady state phase. The profiles have been smoothed, removing effects of sawteeth and Monte Carlo noise.

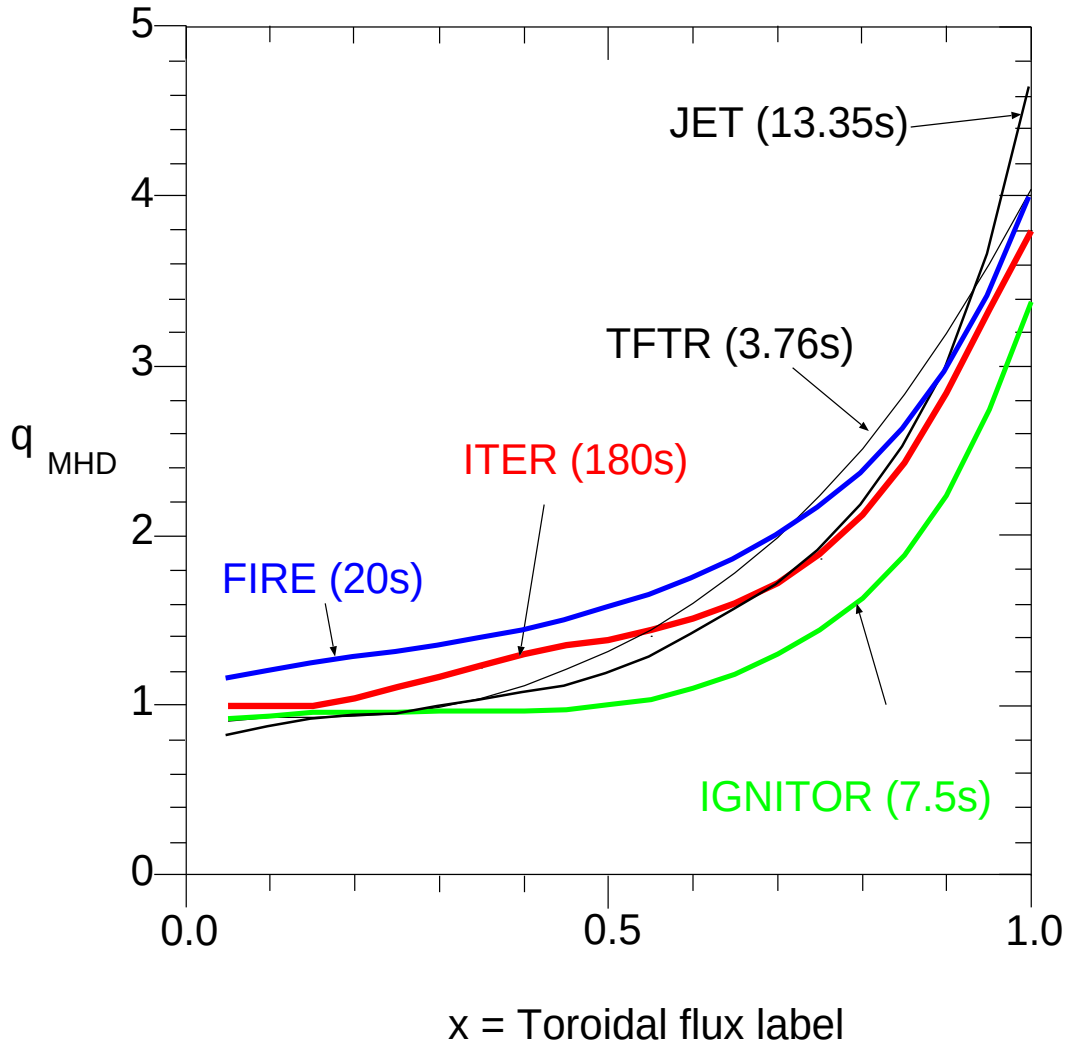

Figure 1. Profiles of q_{MHD} in the TFTR, JET, IGNITOR, FIRE, and ITER plasmas during the steady state phases.

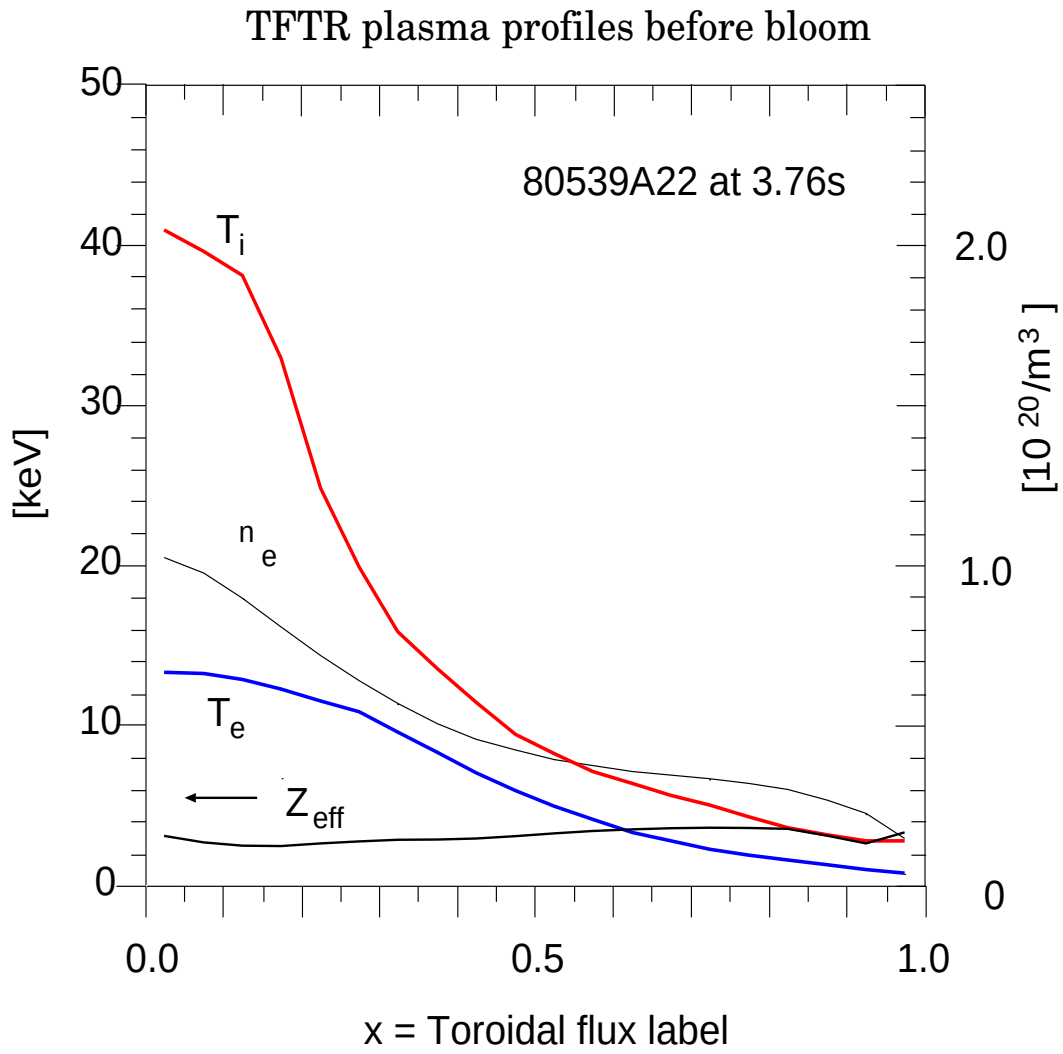

Figure 2. Profiles of the TFTR supershot before the carbon bloom.

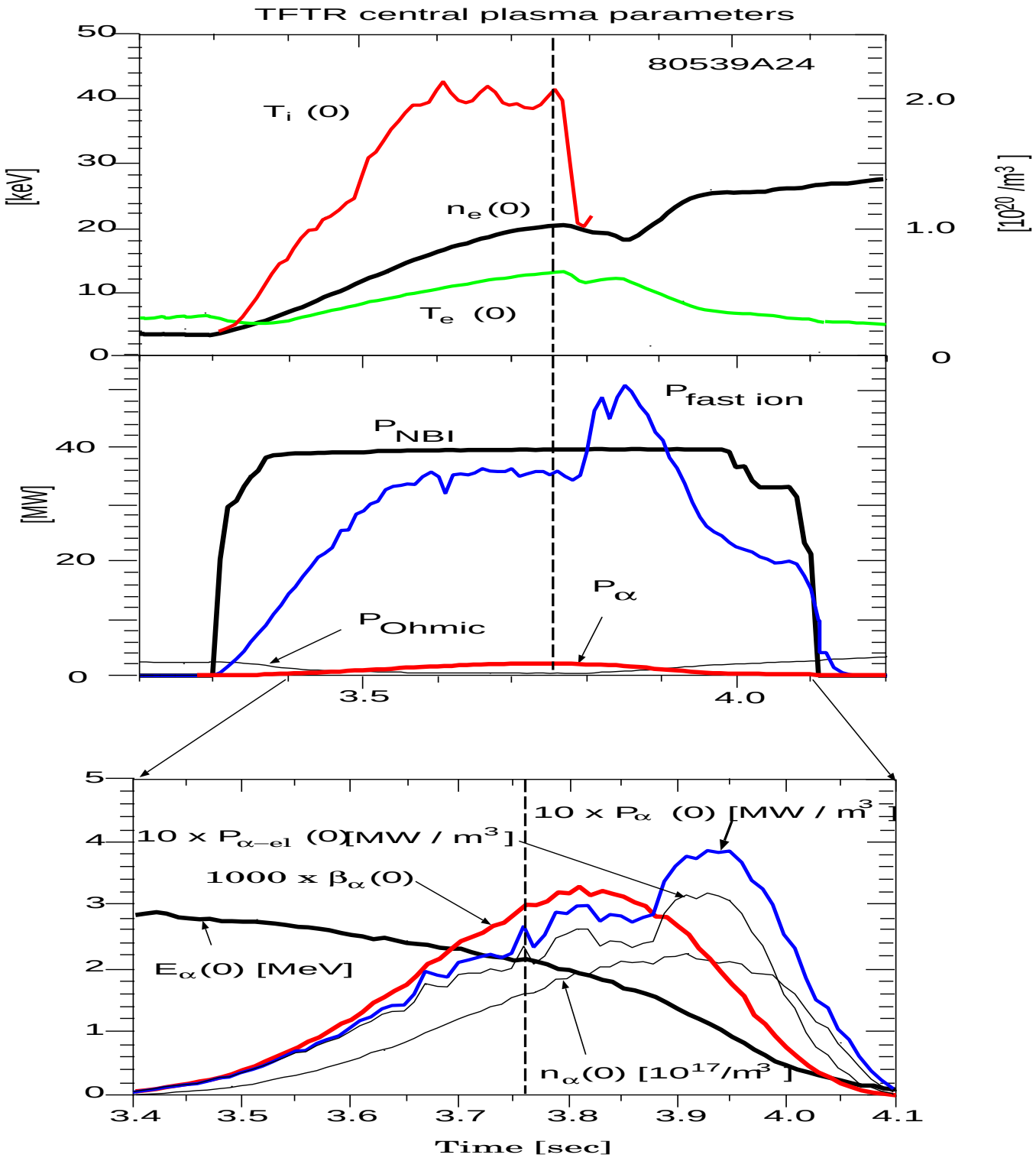

Figure 3. Time evolution of parameters in the TFTR supershot. The charge-exchange-measured T_i profile (for carbon) became hollow with unrealistically low central values after the density became too high for good beam penetration. $P_{fast\ ion}$ is the heating power of the thermal plasma from the NBI and alphas. E_α is the average energy of the fast alphas in the core.

The alpha parameters in c) are volume-averaged out to the $x = 0.1$ flux surface to reduce Monte Carlo fluctuations. The vertical dashed lines indicate the time of the profiles in Fig. 2 (3.76 s).

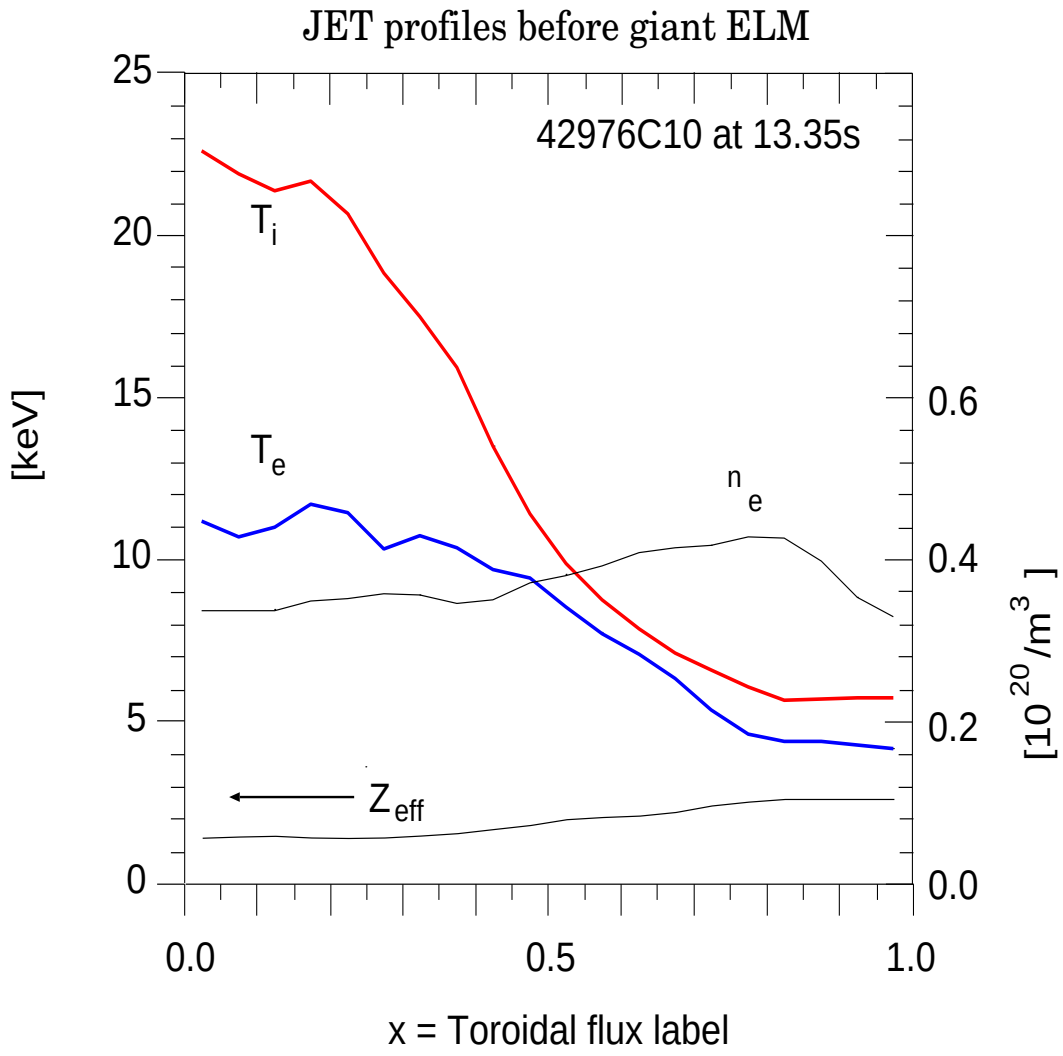

Figure 4. Profiles of the JET hot-ion H-mode plasma before the series of giant ELMs.

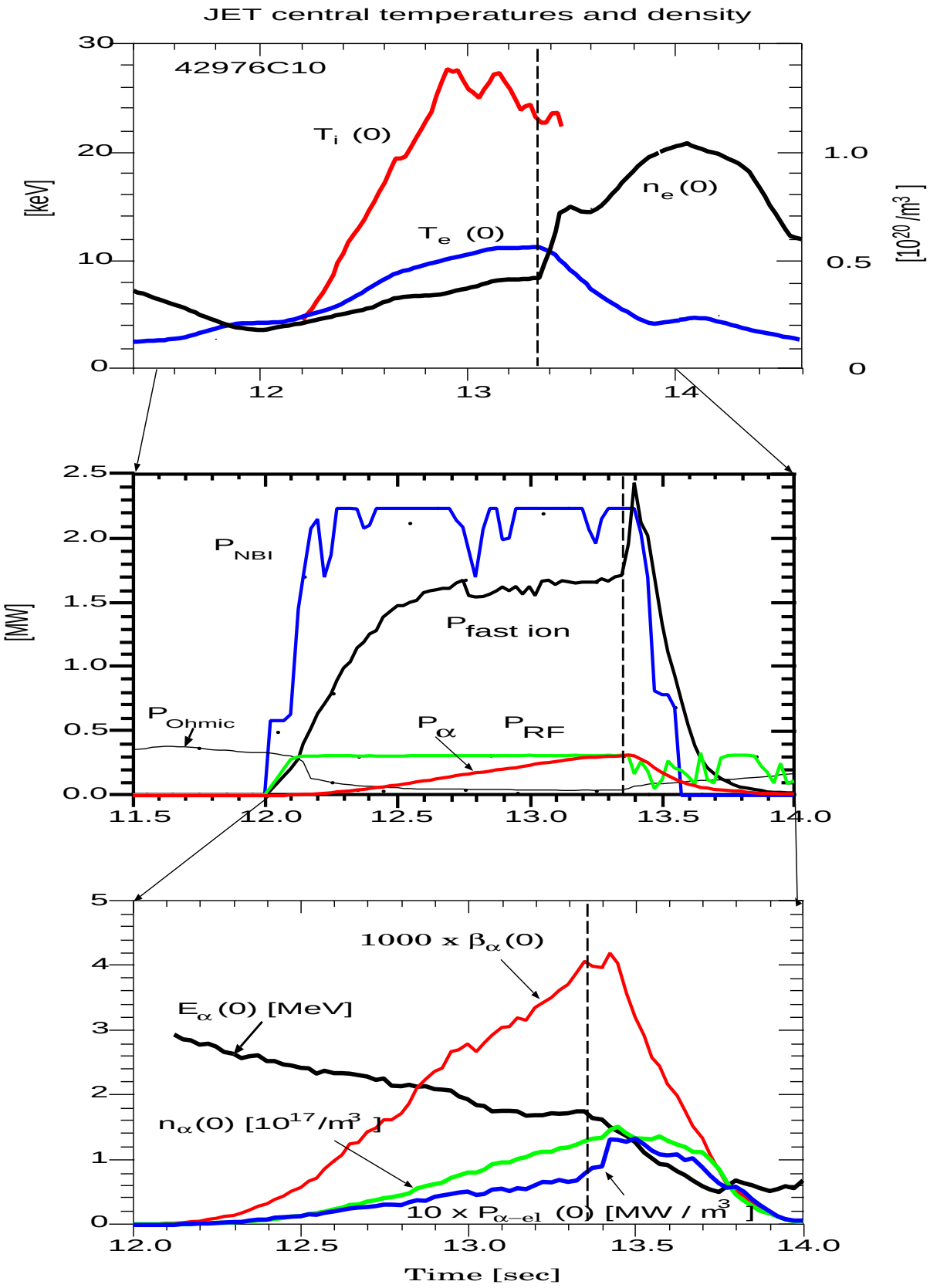

Figure 5. Time evolution of parameters in the JET plasma. The vertical dashed lines indicate the time of the profiles in Fig. 4 (14.35 s).

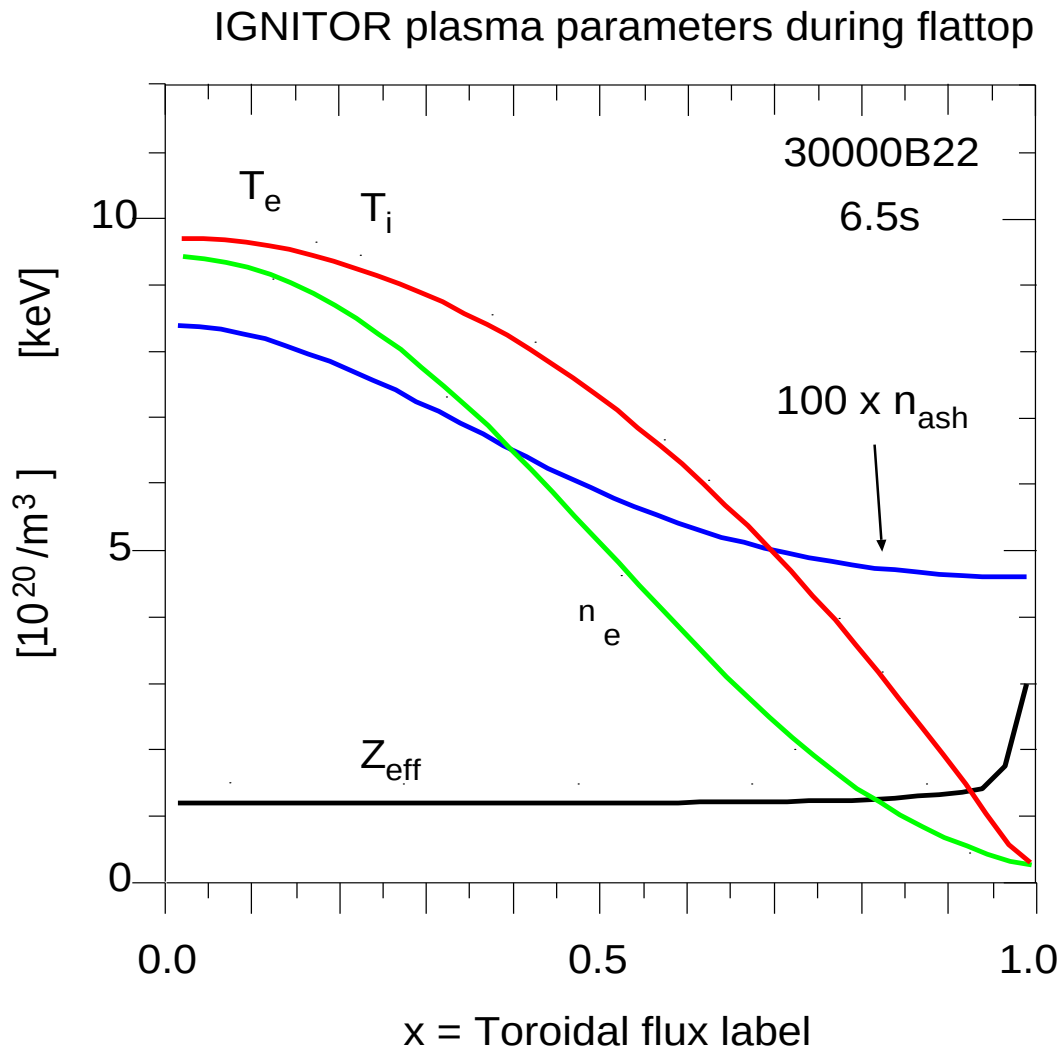

Figure 6. Profiles of the IGNITOR plasma in the flattop phase. The He^4 ash density times 100 is computed from the fast alpha thermalization assuming $R_{ash} = 20\%$ and $D_{ash} = 0.1$ $[m^2/s]$.

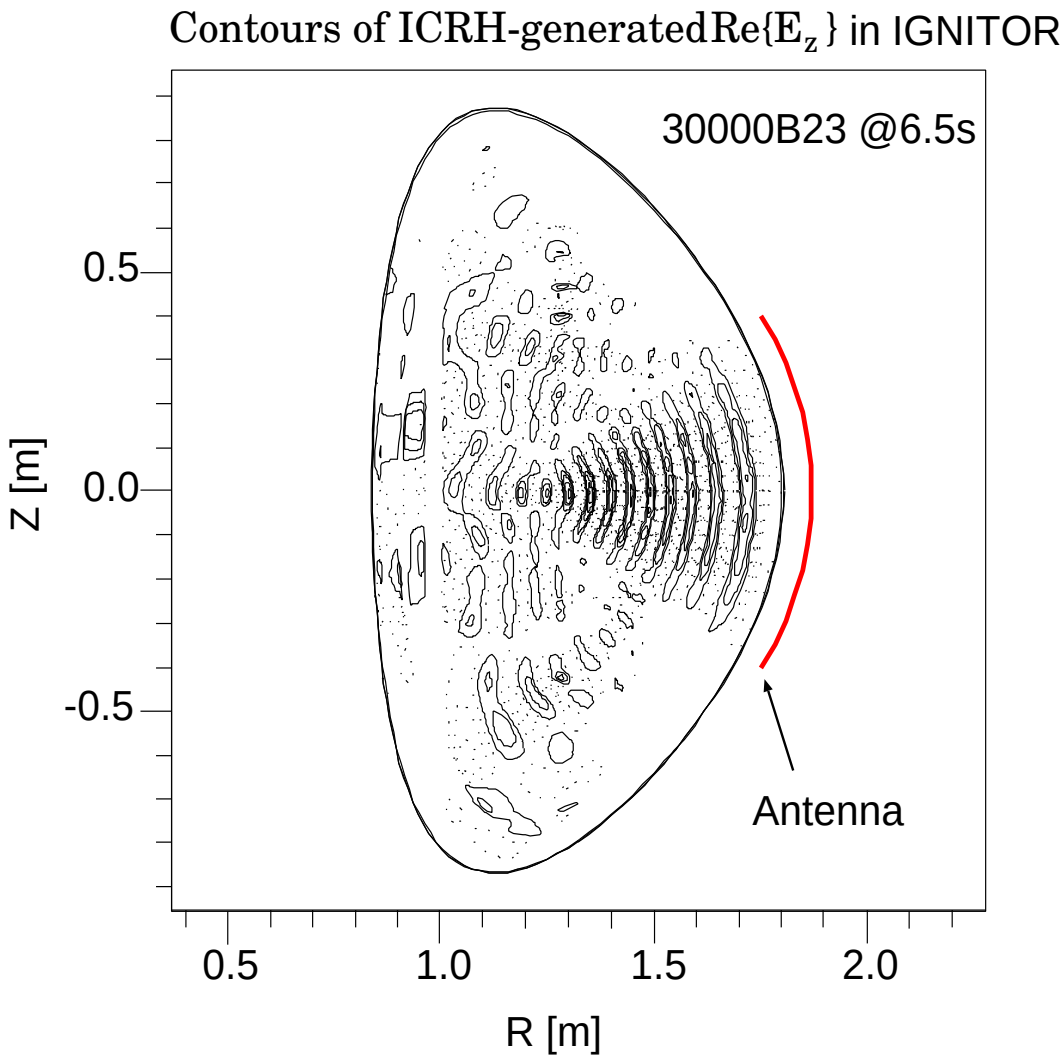

Figure 7. Contours of the 120MHz ICRH-induced Re$\{E_r\}$ in the IGNITOR plasma.

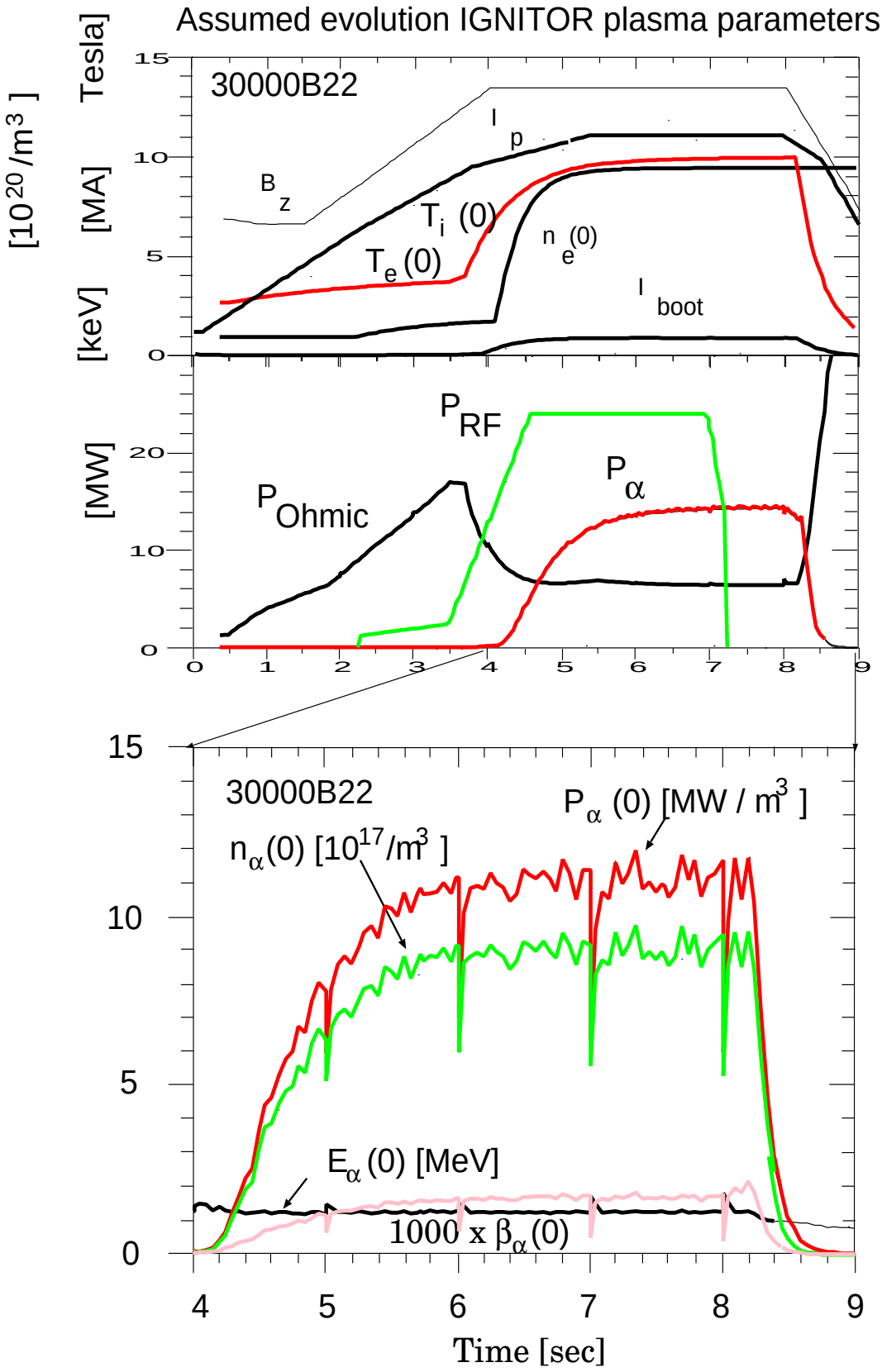

Figure 8. Time evolution of parameters in the IGNITOR plasma.

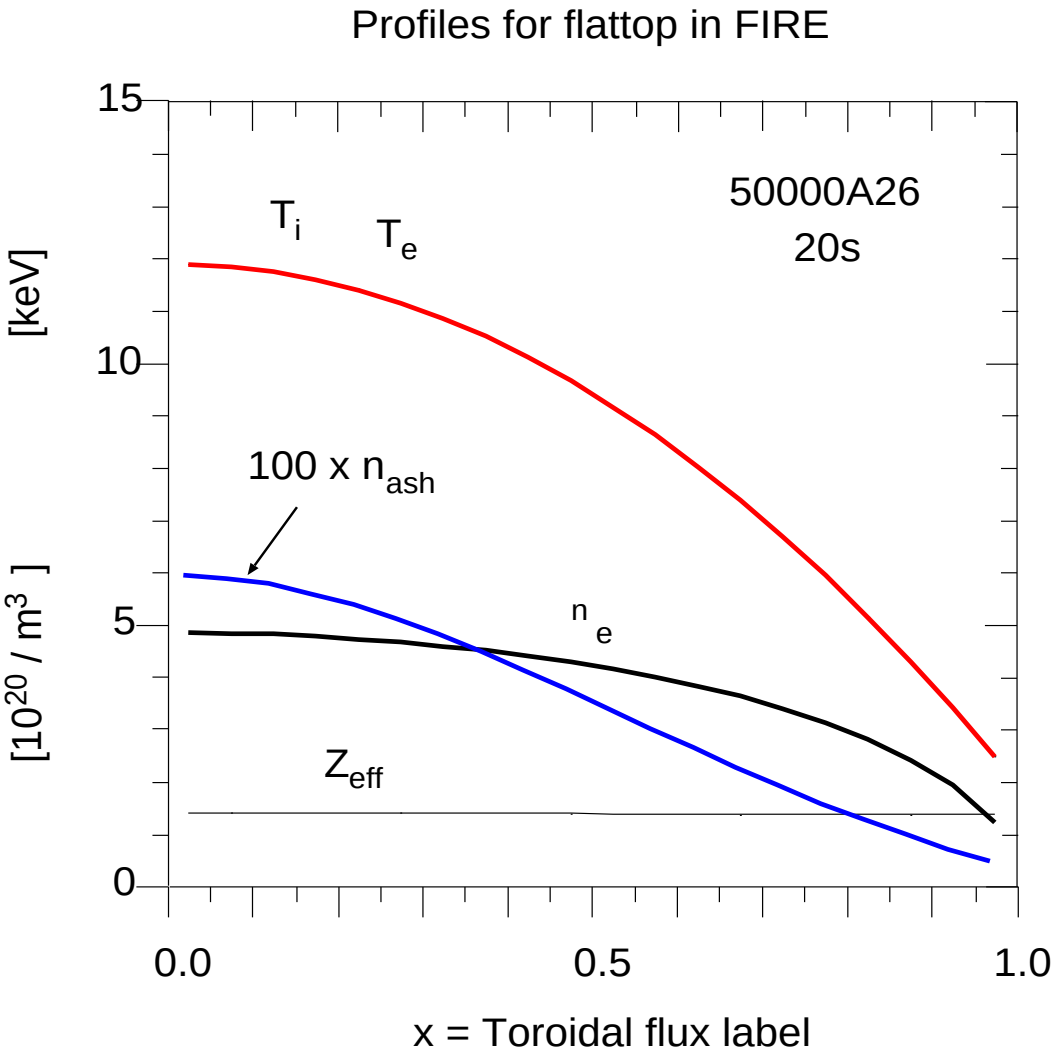

Figure 9. Profiles of the FIRE plasma in the flattop phase. The He^4 ash density times 100 is computed from the fast alpha thermalization assuming $R_{ash} = 20\%$ and $D_{ash} = 0.1$ $[m^2/s]$, and is in steady state at the time shown.

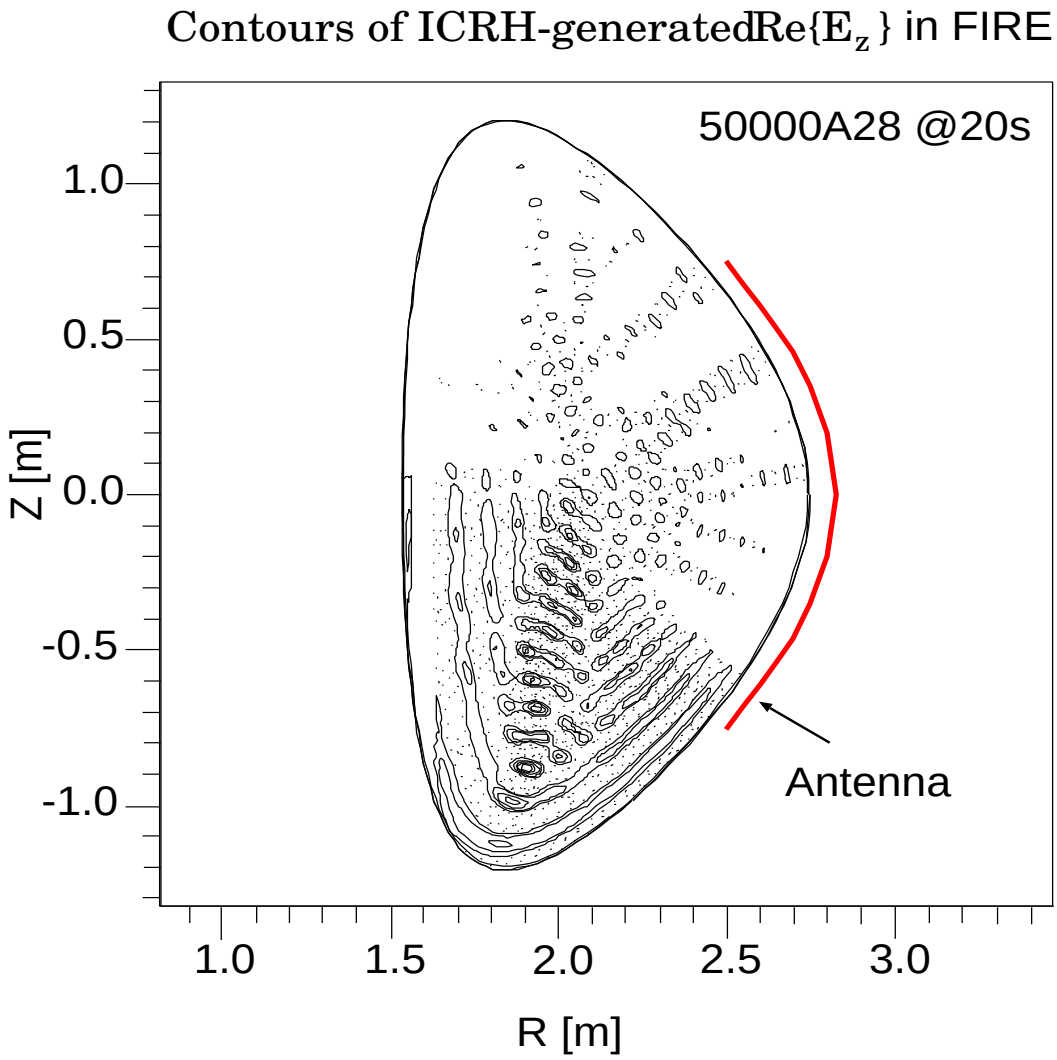

Figure 10. Contours of ICRH-induced Re$\{E_r\}$ in the FIRE plasma.

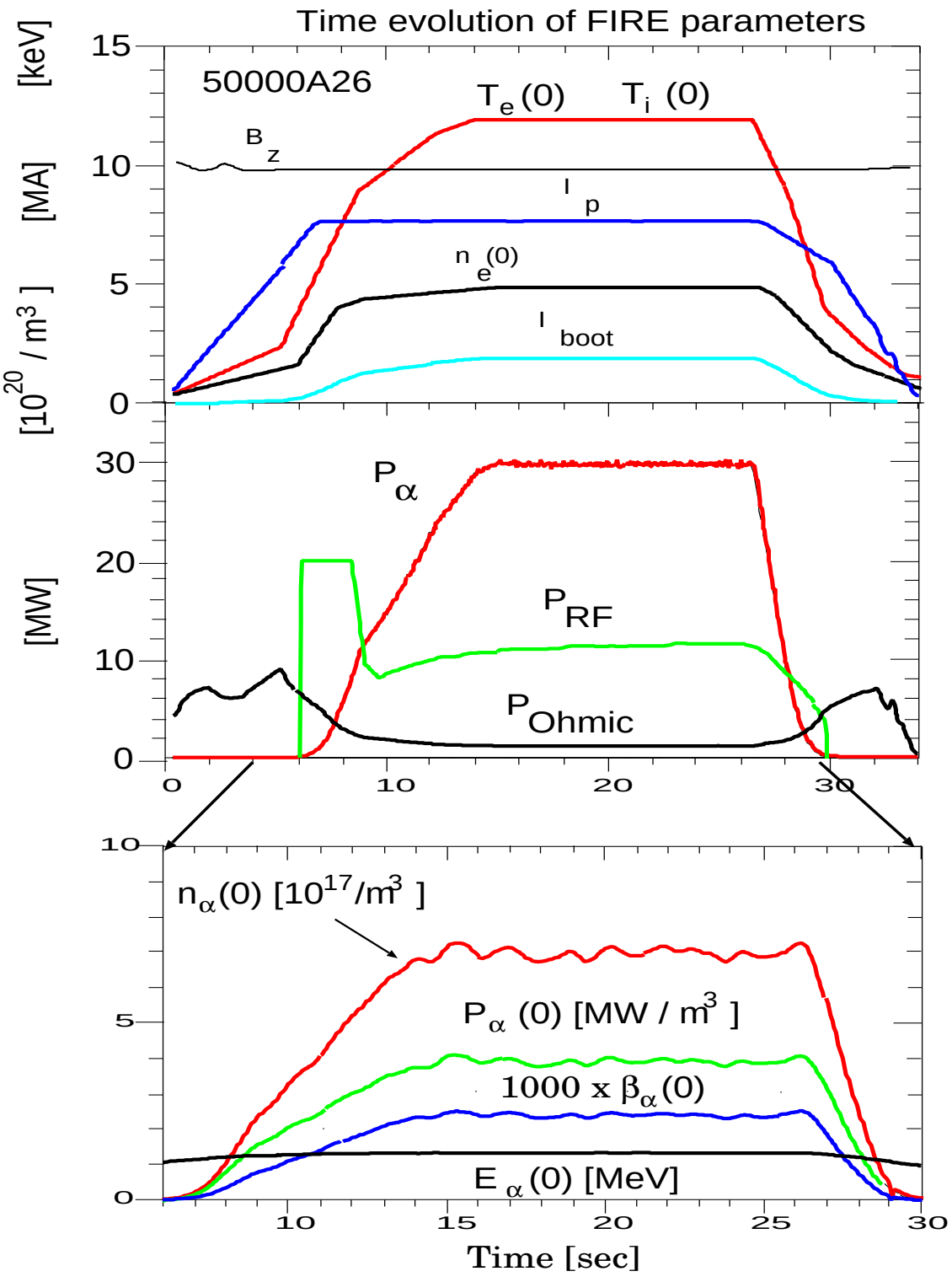

Figure 11. Time evolution of parameters in the FIRE plasma. P_{RF} is high early to obtain the L-H mode transition, then is reduced.

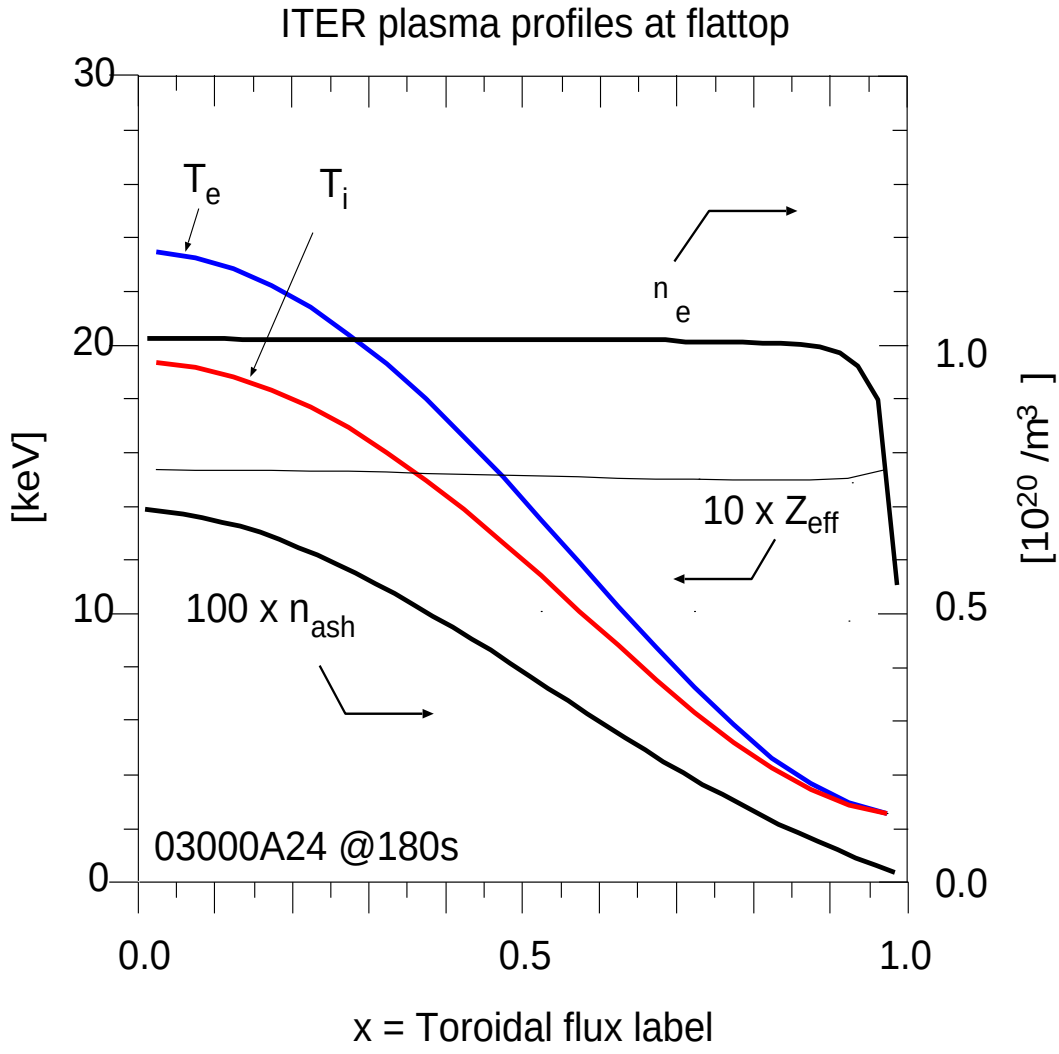

Figure 12. Profiles of the ITER plasma. The He^4 ash density times 100 is computed from the fast alpha thermalization assuming $R_{ash} = 20\%$ and $D_{ash} = 0.8$ $[m^2/s]$, and is in steady state at the time shown.

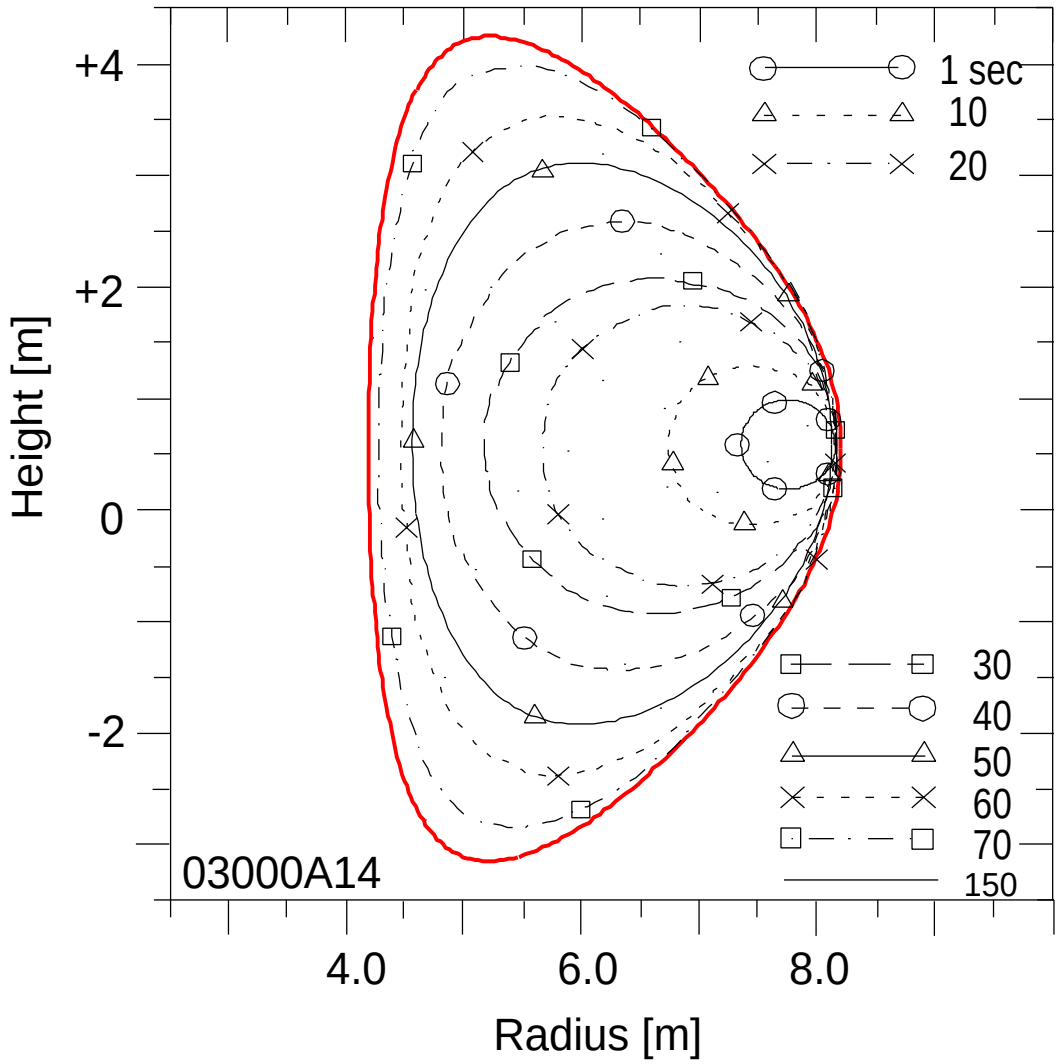

Figure 13. Assumed boundary for the ITER plasma

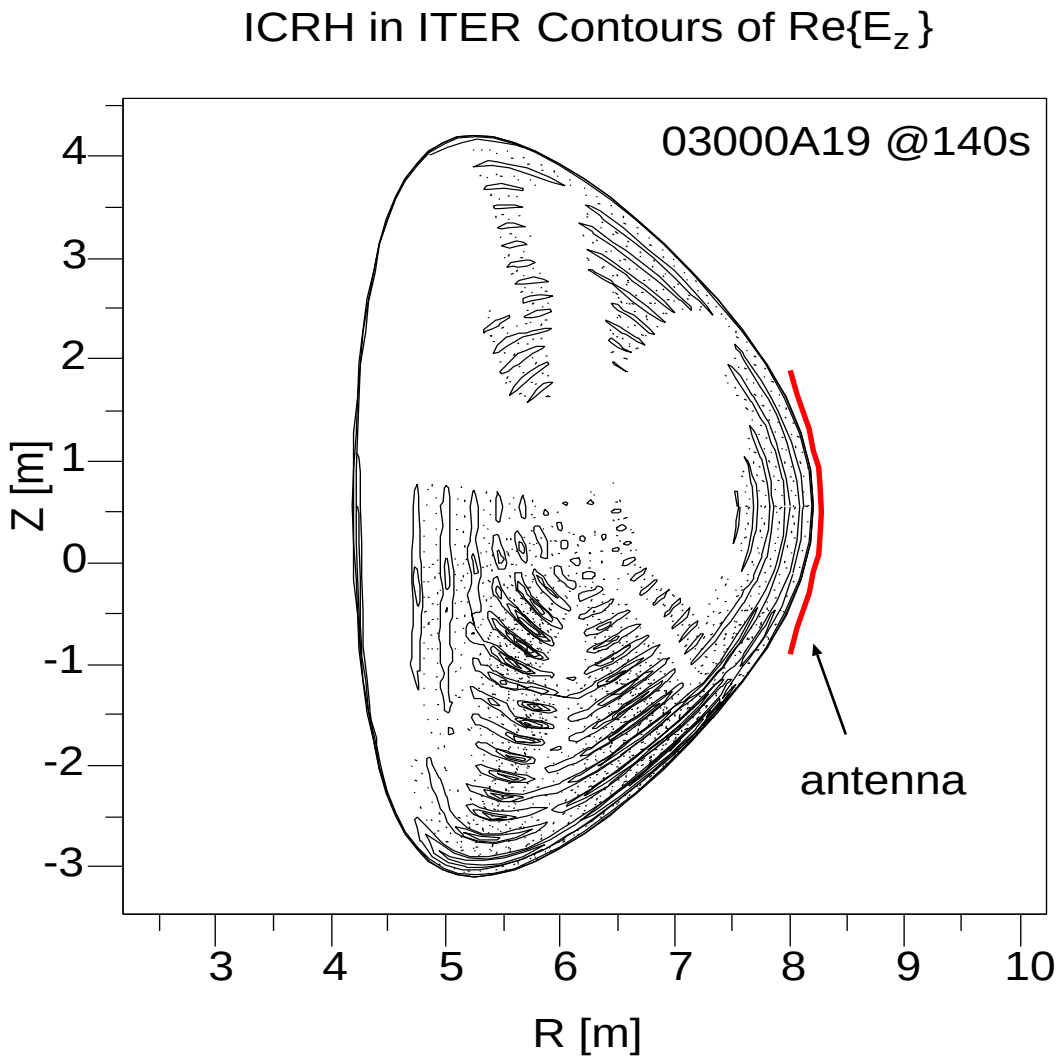

Figure 14. Contours of the ICRH-induced Re$\{E_r\}$ in ITER-FEAT

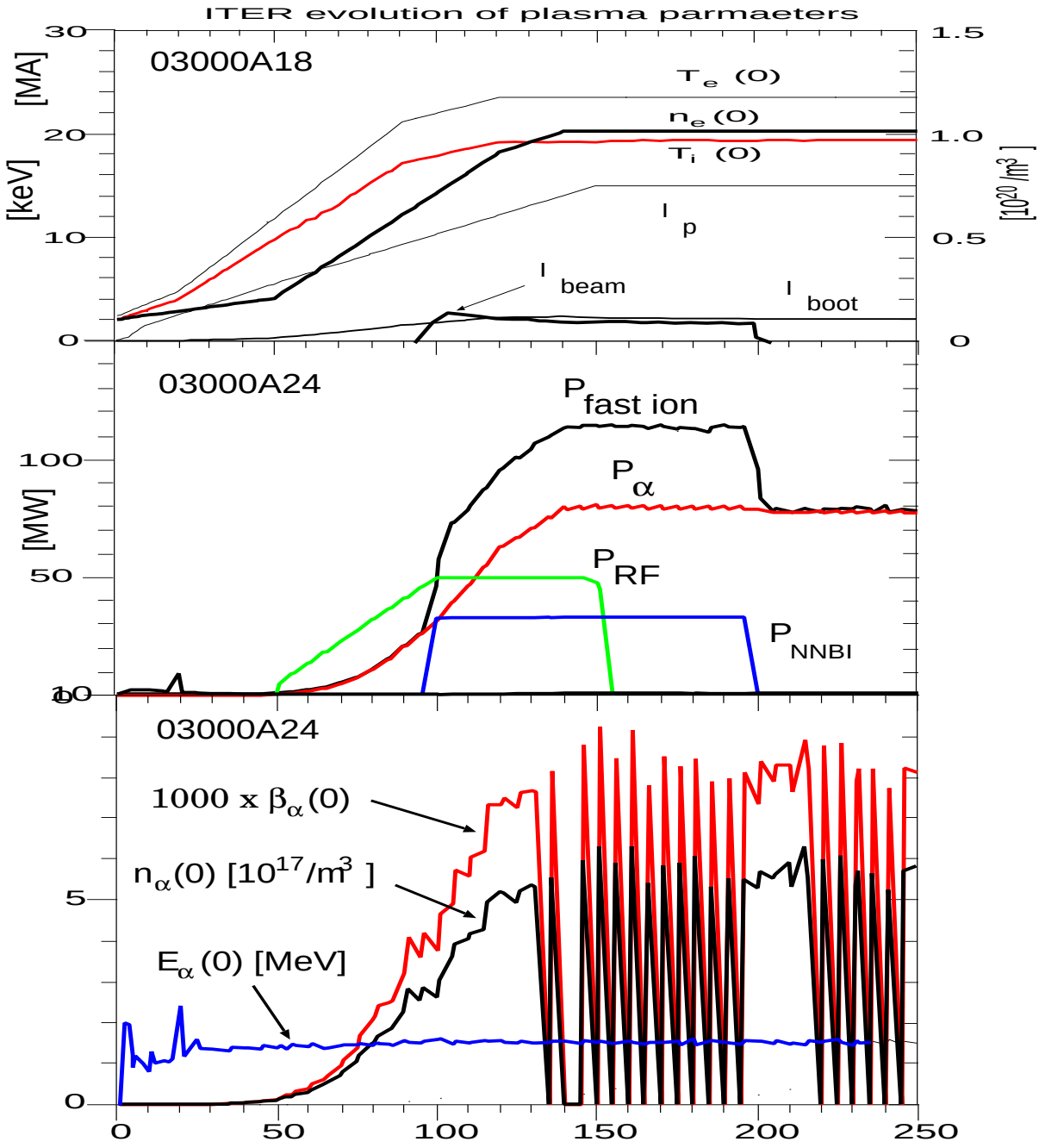

Figure 15. Time evolution of parameters in the ITER baseline scenario. The alpha parameters in c) are volume-averaged out to the $x = 0.1$ flux surface to reduce Monte Carlo fluctuations

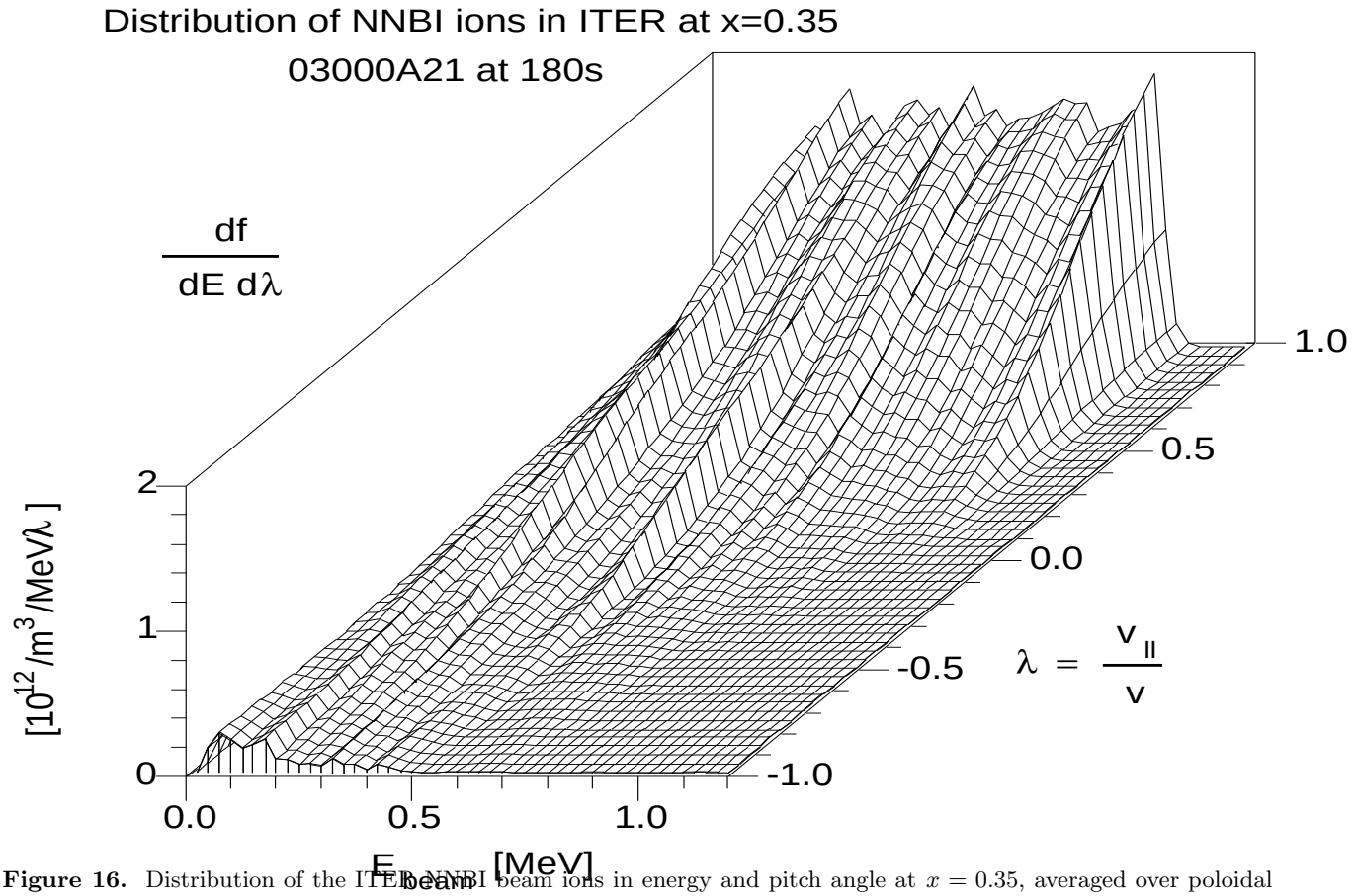

Figure 16. Distribution of the ITER NNBI beam ions in energy and pitch angle at $x = 0.35$, averaged over poloidal angle, computed by the TRANSP Monte Carlo model. The neutrals are injected at 1MeV with $v_\parallel/v = 1$, and the beam ions become more isotropic as they slow down.

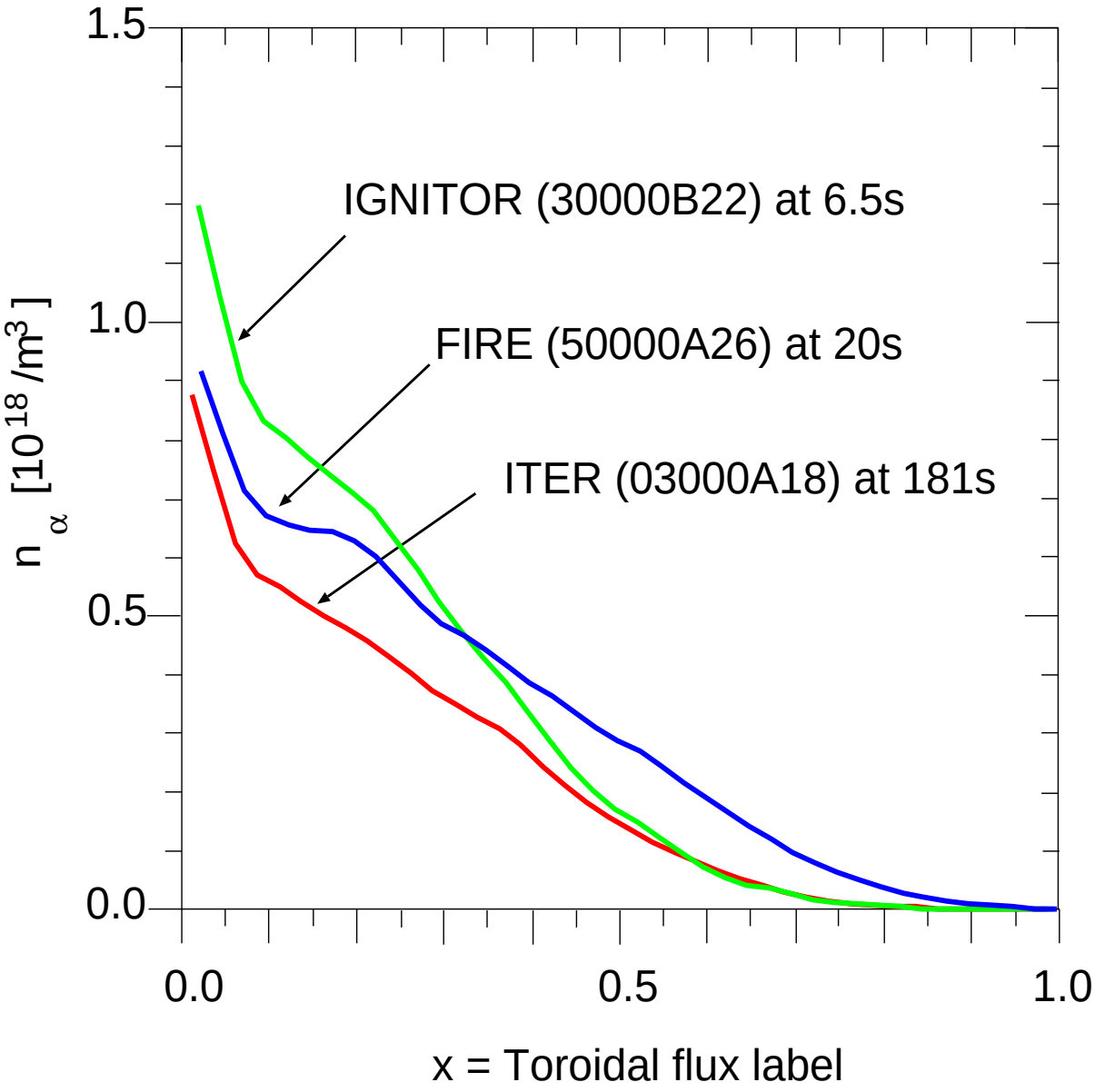

Figure 17. Profiles of the fast alpha densities in IGNITOR, FIRE, and ITER-FEAT during the steady state phase.

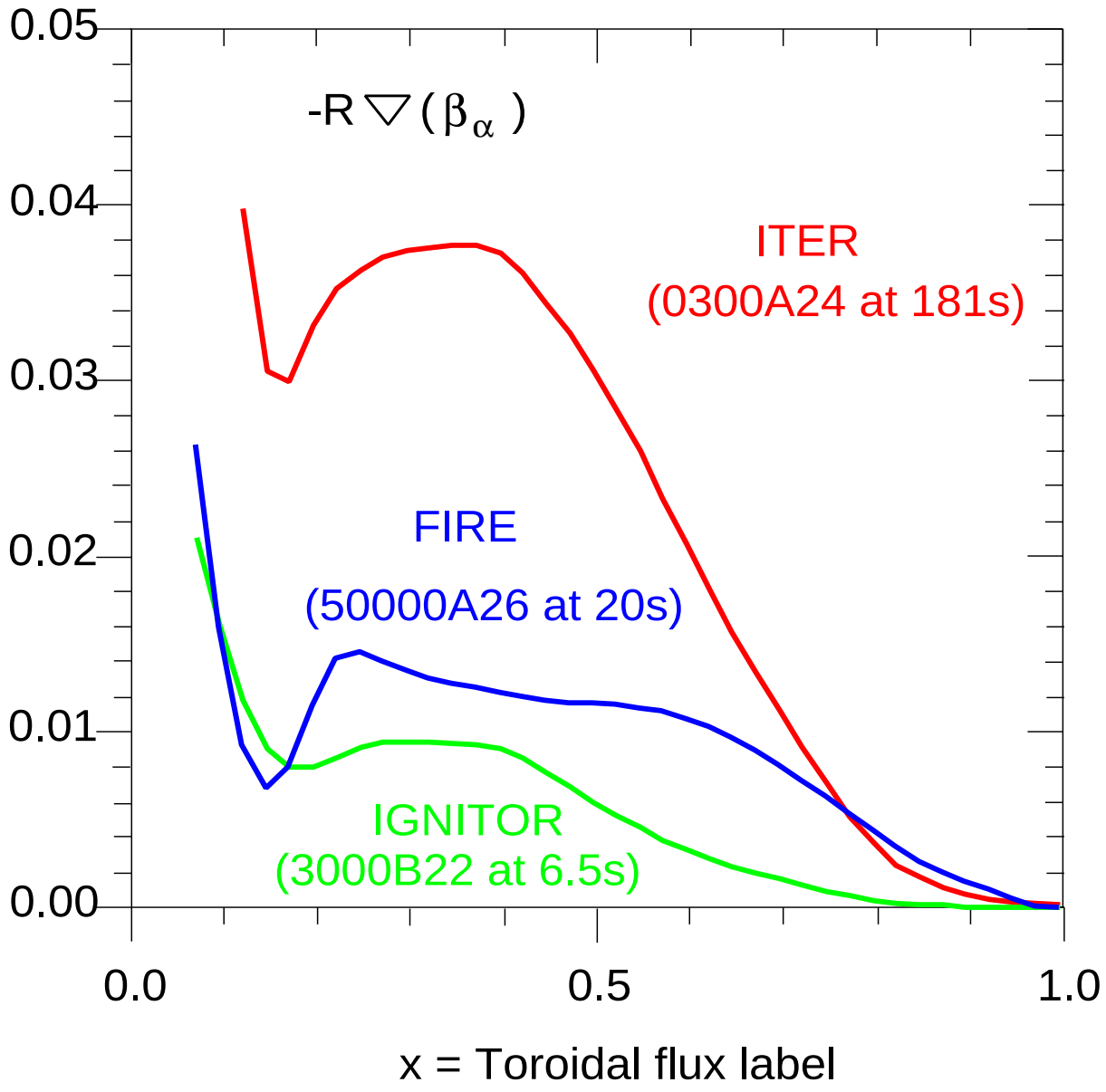

Figure 18. Profiles of $-R \times \nabla(\beta_\alpha)$ in IGNITOR, FIRE, and ITER-FEAT during the steady state phase. The profiles have been smoothed, removing effects of sawteeth and Monte Carlo noise.

External Distribution

Plasma Research Laboratory, Australian National University, Australia
Professor I.R. Jones, Flinders University, Australia
Professor João Canalle, Instituto de Fisica DEQ/IF - UERJ, Brazil
Mr. Gerson O. Ludwig, Instituto Nacional de Pesquisas, Brazil
Dr. P.H. Sakanaka, Instituto Fisica, Brazil
The Librarian, Culham Laboratory, England
Library, R61, Rutherford Appleton Laboratory, England
Mrs. S.A. Hutchinson, JET Library, England
Professor M.N. Bussac, Ecole Polytechnique, France
Librarian, Max-Planck-Institut für Plasmaphysik, Germany
Jolan Moldvai, Reports Library, MTA KFKI-ATKI, Hungary
Dr. P. Kaw, Institute for Plasma Research, India
Ms. P.J. Pathak, Librarian, Insitute for Plasma Research, India
Ms. Clelia De Palo, Associazione EURATOM-ENEA, Italy
Dr. G. Grosso, Instituto di Fisica del Plasma, Italy
Librarian, Naka Fusion Research Establishment, JAERI, Japan
Library, Plasma Physics Laboratory, Kyoto University, Japan
Research Information Center, National Institute for Fusion Science, Japan
Dr. O. Mitarai, Kyushu Tokai University, Japan
Library, Academia Sinica, Institute of Plasma Physics, People's Republic of China
Shih-Tung Tsai, Institute of Physics, Chinese Academy of Sciences, People's Republic of China
Dr. S. Mirnov, TRINITI, Troitsk, Russian Federation, Russia
Dr. V.S. Strelkov, Kurchatov Institute, Russian Federation, Russia
Professor Peter Lukac, Katedra Fyziky Plazmy MFF UK, Mlynska dolina F-2, Komenskeho Univerzita, SK-842 15 Bratislava, Slovakia
Dr. G.S. Lee, Korea Basic Science Institute, South Korea
Mr. Dennis Bruggink, Fusion Library, University of Wisconsin, USA
Institute for Plasma Research, University of Maryland, USA
Librarian, Fusion Energy Division, Oak Ridge National Laboratory, USA
Librarian, Institute of Fusion Studies, University of Texas, USA
Librarian, Magnetic Fusion Program, Lawrence Livermore National Laboratory, USA
Library, General Atomics, USA
Plasma Physics Group, Fusion Energy Research Program, University of California at San Diego, USA
Plasma Physics Library, Columbia University, USA
Alkesh Punjabi, Center for Fusion Research and Training, Hampton University, USA
Dr. W.M. Stacey, Fusion Research Center, Georgia Institute of Technology, USA
Dr. John Willis, U.S. Department of Energy, Office of Fusion Energy Sciences, USA
Mr. Paul H. Wright, Indianapolis, Indiana, USA

The Princeton Plasma Physics Laboratory is operated
by Princeton University under contract
with the U.S. Department of Energy.

Information Services
Princeton Plasma Physics Laboratory
P.O. Box 451
Princeton, NJ 08543

Phone: 609-243-2750
Fax: 609-243-2751
e-mail: pppl_info@pppl.gov
Internet Address: http://www.pppl.gov